REPORT DOCUMENTATION PAGE

AFRL-SR-BL-TR-98-

0689

1. AGENCY USE ONLY *(Leave blank)*	2. REPORT DATE	3. REPORT TYPE AND DATES COVERED
	September 1998	Final Technical Report 15 Apr 96 to 14 Apr 98

4. TITLE AND SUBTITLE
Transport Phenomena Studies By Computational Simulation in Structural Materials Processing

5. FUNDING NUMBERS
F49620-96-C-0015

6. AUTHOR(S)
R. C. Buggeln and M. Meyyappan

7. PERFORMING ORGANIZATION NAME(S) AND ADDRESS(ES)
Scientific Resarch Associates, Inc.
P. O. Box 1058
Glastonbury, CT 06033-1058

8. PERFORMING ORGANIZATION REPORT NUMBER

9. SPONSORING/MONITORING AGENCY NAME(S) AND ADDRESS(ES)
AFOSR/NA
801 North Randolph Street
Arlington, VA 22203-1977

10. SPONSORING/MONITORING AGENCY REPORT NUMBER
F49620-96-C-0015

11. SUPPLEMENTARY NOTES

12a. DISTRIBUTION AVAILABILITY STATEMENT
Approved for Public Release; Distribution Unlimited.

12b. DISTRIBUTION CODE

13. ABSTRACT *(Maximum 200 words)*

Chemical vapor deposition (CVD) is one of the most important techniques for the processing of structural materials. It is extremely versatile in that a wide range of materials and coatings is done by CVD, perhaps more than by any other technique. The process is flexible enough to accommodate a variety of sizes and shapes of objects to be processed and allows continuous change of composition of the material or coating [1]. In this report we discuss the application of CVD processes to 'structural materials'. The classification 'structural materials' here is based on the end use being in aerospace, mechanical and related applications (as opposed to electronics materials) and hence covers coatings and high temperature aerospace materials such as composite structures, ceramic-matrix composites (CMC), functionally-gradient materials (FGM), etc. Representative examples are SiC (fiber, coating), Si3N4, BN, other carbides and nitrides, composites such as SiC-SiC, carbon-SiC, carbon-carbon, and carbon-BN [1].

14. SUBJECT TERMS

15. NUMBER OF PAGES
43

16. PRICE CODE

17. SECURITY CLASSIFICATION OF REPORT	18. SECURITY CLASSIFICATION OF THIS PAGE	19. SECURITY CLASSIFICATION OF ABSTRACT	20. LIMITATION OF ABSTRACT
Unclassified	Unclassified	Unclassified	UL

TRANSPORT PHENOMENA STUDIES BY COMPUTATIONAL SIMULATION IN STRUCTURAL MATERIALS PROCESSING

R.C. Buggeln and M. Meyyappan
Scientific Research Associates, Inc.
P.O. Box 1058
Glastonbury, CT 06033-1058

September 1998

Air Force Office of Scientific Research
STTR Contract F49620-96-C-0015
(860) 659-0333

Table of Contents

• INTRODUCTION

Chemical vapor deposition (CVD) is one of the most important techniques for the processing of structural materials. It is extremely versatile in that a wide range of materials and coatings is done by CVD, perhaps more than by any other technique. The process is flexible enough to accommodate a variety of sizes and shapes of objects to be processed and allows continuous change of composition of the material or coating [1]. In this report we discuss the application of CVD processes to 'structural materials'. The classification 'structural materials' here is based on the end use being in aerospace, mechanical and related applications (as opposed to electronics materials) and hence covers coatings and high temperature aerospace materials such as composite structures, ceramic-matrix composites (CMC), functionally-gradient materials (FGM), etc. Representative examples are SiC (fiber, coating), Si_3N_4, BN, other carbides and nitrides, composites such as SiC-SiC, carbon-SiC, carbon-carbon, and carbon-BN [1].

There are several variations of CVD in the preparation of structural materials. These include:

(1) CVD coating of complex arbitrary shapes and internal cavities such as occur in the following examples. Hard CVD coatings are used in rocket nozzles and gas turbine engines for erosion and wear resistance. TiB_2 and TiC coatings are used for coating titanium blades and Si_3N_4 coatings on carbon nozzles. Al_2O_3, TiN, TiC and TiB_2 coatings are used on tool bits to increase the cutting life of tools through improvements in hardness and wear resistance. CVD metal films are used as protective coatings.

(2) Conventional CVD on substrates: This offers a proven method for producing dense crystalline materials for a variety of applications; monolithic ceramic materials such as SiC, TiC, boron; ceramic materials as diffusion barriers.

(3) CVD of fibers. Examples include SiC, Si_3N_4, boron, and oxide fibers. These monofilament fibers are used primarily for reinforcing other materials in producing desirable composites.

(4) CVD of preforms. Here the CVD process is used to infiltrate a preform made from one of the above fibers to form a composite. CVD inside preforms is generally called chemical vapor infiltration (CVI). Composites such as SiC-SiC, C-C, C-SiC, and C-BN have been produced by this technique.

(5) Plasma-based CVD. This variation allows lower processing temperatures that may be critical in some applications to obtain the desired microstructures. While it is popular in semiconductor processing, plasma-based CVD has been recently considered in processing of structural materials.

Materials processed by CVD have found a large number of applications in aerospace, automotive, mechanical, and related industries. In addition to the applications mentioned above other applications include SiC produced by CVD. SiC produced by CVD alone commands a range of applications. For example, CVD-grown SiC is used for high temperature engineering applications such as reaction tubes, furnace components and liners, heating elements, and refractory ware. CVD SiC is a good candidate for materials that must withstand severe environments. This includes transmissive domes in high-speed missiles, reflective and transmissive optical components, UV telescopes and instruments for astronomy and chemically inert industrial seals. SiC is also attractive for storage media heads and disks for high packing density, and finally, in semiconductor device applications.

Carbon-carbon composites are used in rocket nozzles, nose cones for re-entry vehicles, heat shields, and aircraft brakes [2]. SiC-SiC and C-SiC find many high temperature applications. ZrO_2 composite reinforced with TiN whiskers is a good candidate for advanced heat engines due to a good match of thermal properties. In producing some composites, improvements in reliability and performance can be expected when such materials are designed with a continuous compositional, and therefore, functional gradient. In summary, application for CVD-grown materials is rather extensive and it is not an overstatement to say that the related commerce including end uses (both structural and electronics) can be measured in billions of dollars.

Despite the impressive range of applications outlined above, a fundamental understanding of CVD of structural materials is lacking. A recent National Research Council report [3] on high performance composites, prepared by a distinguished panel for the National Materials Advisory Board, states: "A basic science approach to the CVD..., providing fundamental insights into decomposition kinetics, fiber-formation mechanisms, and surface reactions, can result in a better optimization of processes and products. Although it may not be inordinately difficult to form a new CVD fiber of a given composition initially, achievement of consistency in properties may require understanding and carefully controlling the parameters of the deposition process."

The above conclusion is even more valid when the composition is varied to produce FGMs. In addition, process scale-up from laboratory to large scale manufacturing is difficult because of the complexity of the CVD process which is characterized by the simultaneous heat, momentum and mass transfers along with gas phase (homogeneous) and surface (heterogeneous) reactions and complex flow-induced orientation effects. In this regard, mathematical modeling of the transport phenomena associated with the process, and computer simulation is valuable in many respects, including:

(1) providing an understanding of the process mechanisms;

(2) developing a cause and effect relationships between the process variables (for which there are knobs on the reactor panel) vs. process figures-of-merit, such as growth rate, uniformity, surface material composition, etc. (note that these figures-

of-merit, in turn, affect the structural characteristics, including mechanical and thermal properties);

(3) process optimization to meet production goals;

(4) equipment design to meet given processing objective; and

(5) process control.

Although models and computer code can serve as a cost-effective design tool, to date there has been very little modeling work for CVD of composites. This lack of application results from a variety of issues regarding physical models and computational techniques that must be resolved to allow practical application of state-of-the-art computational tools to the problem of CVD formed composites. These include:

- models for multi-component mass transfer with chemical reactions in composites processing,
- surface reactions and related surface phenomena,
- sound models for thermal diffusion,
- preform infiltration,
- model to represent the random pore network of the preforms,
- development of suitable boundary conditions,
- transient analysis to study growth of FGMs
- computational techniques appropriate for the above physical processes both in terms of simulation speed and accuracy, and
- models to correlate the transport phenomena effects to the microstructure, mechanical, and thermal properties.

The Small Business Technology Transfer (STTR), that is reported herein, addresses these issues as it develops suitable transport and reaction models for CVD and CVI of composites within the framework of a computational simulation tool. This work has significant relevance to Air Force missions since high temperature composites are extensively used in military applications. Affordability and reliability of materials are two ultimate factors that determine the success of modern weapon systems. In general, the required materials are very specialized, low volume, and come with stringent specifications. Improved processes through a better understanding provided by modeling will impact on the material quality and cost of processing.

•ANALYSIS

CVD Processes

Modeling of the CVD processes require solution of the appropriate governing equations, specification of appropriate boundary conditions, specification of mathematical models of relevant physical process and an efficient and accurate solution procedure. Those developed and used in the present effort are discussed in this Section.

Governing Equations

At pressures and temperatures normally used in CVD of structural materials, the mean free path of the gas molecules is much smaller than the reactor dimensions and as such, a continuum analysis is appropriate to study the transport and kinetics inside the reactor. The following are the global mass, momenta, energy and individual species mass conservation equations, respectively.

$$\frac{\partial \rho}{\partial t} + \nabla \cdot \rho \mathbf{U} = 0 \tag{1}$$

$$\frac{\partial \rho \mathbf{U}}{\partial t} + \nabla \cdot \rho \mathbf{U}\mathbf{U} = -\nabla P + \nabla \cdot \tau + \rho \mathbf{g} \tag{2}$$

$$\frac{\partial \rho h}{\partial t} + \nabla \cdot \rho h \mathbf{U} = -\nabla \cdot \mathbf{q} + \frac{DP}{Dt} + \Phi + \mathbf{Q}_{ext} \tag{3}$$

$$\frac{\partial \rho \omega_i}{\partial t} + \nabla \cdot \rho \omega_i \mathbf{U} = -\nabla \cdot \mathbf{j}_i + \sum_{j=1}^{J} R_{i,j} \qquad (i = 1,N) \tag{4}$$

where ρ is the total density, $\mathbf{U}$ is the mass-averaged gas velocity, P is the pressure, τ is the viscous stress tensor and $\mathbf{g}$ is the gravitational vector. h is the static enthalpy, $\mathbf{q}$ is the total energy flux relative to mass average velocity (i.e., diffusional energy flux) and Φ is the mean flow dissipation rate. Q_{ext} represents external heat sources including radiation. $\mathbf{j}_i$ is the diffusive mass flux of the i^{th} species and $\omega_i = \rho_i / \rho$ is the mass fraction of the i^{th} species. The last term in Eq. (4), $\sum_{j=1}^{J} R_{i,j}$, represents the i^{th} species mass production or loss through the J homogeneous chemical reactions.

The above transport equations need to be augmented with an equation of state, viz., the perfect gas law.

$$P = \frac{\rho R T}{M} \tag{5}$$

where T is the gas temperature and R is the universal gas constant. Here the mixture molecular weight, M, is given by

$$M = \frac{1}{\sum_{i=1}^{N} \frac{\omega_i}{M_i}} \tag{6}$$

where N is the number of gaseous species and M_i is the molecular weight of the i^{th} species. Further details on some of the key terms in the above equations are given below.

The static enthalpy per unit mass, h, is the mixture enthalpy of N species,

$$h = \sum_{i=1}^{N} \omega_i h_i(T) \tag{7}$$

where $h_i(T)$ is the enthalpy per unit mass of the i^{th} species (a function of temperature only). The temperature, T, is related to enthalpy, h, via the relationship

$$h = \sum_{i=1}^{N} \omega_i \left[h_{f_i} + \int_{T_{f_i}}^{T} C_{p_i}(T')\,dT' \right] \tag{8}$$

where h_{f_i} is heat (enthalpy) of formation of the i^{th} species at temperature T_{f_i} and $C_{p_i}(T')$ is the specific heat at constant pressure for the i^{th} species.

The total energy flux, $\mathbf{q}$, is the sum of the conductive (Fourier) and inter-diffusional contributions, $\mathbf{q}_c$ and $\mathbf{q}_d$, respectively where

$$\mathbf{q}_c = -\kappa \nabla T \tag{9}$$

$$\mathbf{q}_d = \sum_{i=1}^{N} h_i(T)\mathbf{j}_i \tag{10}$$

Here κ is thermal conductivity.

The viscous stress tensor, τ, is related to the rate of strain tensor, $\mathbf{D}$, and the molecular viscosity, μ, by the relationship

$$\tau = \mu \left[2\mathbf{D} - \frac{2}{3}(\nabla \cdot \mathbf{U})\delta \right] \tag{11}$$

where

$$\mathbf{D} = \frac{1}{2}\left(\nabla \mathbf{U} + \nabla \mathbf{U}^{\mathrm{T}}\right) \tag{12}$$

where the superscript T refers to the transpose. The dissipation, Φ, is given by

$$\Phi = 2\mu\,\mathbf{D}:\mathbf{D} - \frac{2}{3}\mu\left(\nabla\cdot\mathbf{U}\right)^2 \tag{13}$$

For the results reported in this study, the Reynolds numbers were sufficiently low enough that the effects of turbulence were negligible. Thus the Reynolds stress terms were neglected.

Molecular Properties

For the cases of interest in this study the gases consist of mixtures of individual gaseous species. Therefore it was necessary to calculate multiple species values of viscosity, diffusivity and thermal conduction. The models used are discussed in detail in [4] and [5]. For the mixture viscosity, μ, the semi-empirical formula of Wilke was used, viz.,

$$\mu = \sum_{i=1}^{N} \frac{x_i \mu_i}{\sum_{j=1}^{N} x_j \phi_{ij}} \tag{14}$$

where $x_i = \omega_i M / M_i$ is the mole fraction of the i^{th} species, μ_i is the molecular viscosity of the i^{th} species at the specified temperature and pressure and

$$\phi_{ij} = \frac{\left[1 + \left(\frac{\mu_i}{\mu_j}\right)^{\frac{1}{2}} \left(\frac{M_j}{M_i}\right)^{\frac{1}{4}}\right]^2}{\sqrt{8\left(1 + \frac{M_i}{M_j}\right)}} \tag{15}$$

The individual species viscosity, μ_i, is calculated from Chapman-Enskog kinetic theory by

$$\mu_i = \frac{\frac{5}{16\pi}\sqrt{\frac{\pi k M_i T}{N_0}}}{\sigma_i^2\,\Omega_\mu\left(T^*\right)} \tag{16}$$

where k is Boltzmann's constant and N_0 is Avogadro's number and the reduced temperature, T^*, is given by

$$T^* = \frac{kT}{\varepsilon_i} \tag{17}$$

where σ_i and ε_i are know (measured constants) for each species. $\Omega_\mu(T^*)$ is the Lennard-Jones potential for viscosity.

The mixture thermal conductivity, κ, is calculated by a relationship similar to Eq. (14)

$$\kappa = \sum_{i=1}^{N} \frac{x_i \kappa_i}{\sum_{j=1}^{N} x_j \phi_{ij}} \tag{18}$$

where κ_i is the i^{th} species thermal conductivity and is calculated from Euken's formula

$$\kappa_i = \left(C_{p_i}(T) + \frac{5R}{4M_i} \right) \mu_i \tag{19}$$

Finally calculation of the diffusive fluxes requires the evaluation of the binary diffusion coefficients, D_{ij}. In this analysis the Chapman-Enskog formulation is used

$$D_{ij} = \frac{\frac{3}{8}\sqrt{\frac{\pi k^3 N}{2}}\sqrt{T^3\left(\frac{1}{M_i}+\frac{1}{M_j}\right)}}{P\sigma_{ij}\Omega_D(T^*)} \tag{20}$$

where

$$T^* = \frac{kT}{\varepsilon_{ij}} \tag{21}$$

and the Lennard-Jones parameters, σ_{ij} and ε_{ij} are given by

$$\sigma_{ij} = \frac{1}{2}(\sigma_i + \sigma_j) \tag{22}$$

and

$$\varepsilon_{ij} = \sqrt{\varepsilon_i \varepsilon_j} \tag{23}$$

and Ω_D (T^*) is the Lennard-Jones potential for diffusion. It is to be noted that D_{ij} is symmetric, i.e., $D_{ij} = D_{ji}$.

Multi-component Diffusive Flux Model

The diffusive term $\mathbf{j}_i$ in Eq. (4) consists of three contributions: (1) diffusion due to concentration gradient (ordinary diffusion), (2) diffusion due to temperature gradient (Soret or thermal diffusion), and (3) diffusion due to pressure gradients (neglected in this study). If only two components are present, the ordinary diffusive flux for two components, i and j, are given by Fick's law.

$$\mathbf{j}_i = -\rho D_{ij} \nabla \omega_i \tag{24}$$

where D_{ij} is the binary diffusivity of i into j. If the carrier gas is the major component and all active species are small fractions, then the mixture may be considered dilute. In this case, each active species may be thought of as diffusing into the carrier gas, and the corresponding binary diffusivity is an appropriate approach. However, when no dominant carrier gas is present or when the carrier gas is a light molecule such as hydrogen or helium, the dilute species approximation is not appropriate. It is then necessary to consider multi-component mass transfer. Multi-component mass transfer is described by the Stefan-Maxwell equations. Since solution of the Stefan-Maxwell equations is very difficult and time consuming, in practice an effective multi-component diffusivity for the i^{th} species into the mixture D_i is defined. The definition of D_i is:

$$D_i = \frac{1 - x_i}{\sum_{\substack{j=1 \\ j \neq i}}^{N} \frac{x_j}{D_{ij}}} \tag{25}$$

Here x_i is the mole fraction. It is noted that diffusive fluxes of all species must sum up to zero, i.e., $\sum_{i=1}^{N} j_i = 0$; only then would all species conservation equations sum to give the global mass continuity Eq. (1). With the form of Eq. (24), this condition is realizable in practice if all the diffusion coefficients are equal; but this constraint is too restrictive. While different approaches may be used to satisfy the above constraint, a rigorous procedure yields

$$\mathbf{j}_i = -\frac{\rho}{M} D_i \nabla(\omega_i M) + \omega_i \sum_{j=1}^{N} \frac{\rho D_j}{M} \nabla(\omega_j M) \tag{26}$$

as shown by Ramshaw [6,7]. Though expression (26) is significantly more complex than expression (24), it yields zero net diffusive flux for arbitrary D_i and D_j and thus conserves

mass. This approach is better than that often used in the literature and in those commercial codes where the expression in Eq. (24) is used.

Another issue of concern when expression (24) is used instead of (26) is that usually one of the species from the set of N is not solved, and its mass or mole fraction is obtained by subtracting the sum of the other N-1 species from unity. This is not only subject to round-off errors, but also may result in an "asymmetric" situation, wherein the final results may depend on which species is not determined directly from its species conservation equation.

Thermal Diffusion Model

In CVD applications thermal (Soret) diffusion often may be an important component of the diffusion process. The thermal diffusion flux is given by

$$j_{i,T} = -D_{i,T}\nabla(\ln T) \tag{27}$$

Here, $D_{i,T}$ is the thermal diffusion coefficient for the i^{th} species. Modelers generally rely on empirical relations or data to evaluate $D_{i,T}$. For many species of interest in structural materials processing, such data are not available. The present approach is a first-principles-based procedure based upon the approach described by Ramshaw [6,7]. $D_{i,T}$ is written in the form

$$D_{i,T} = \frac{D_i}{M} M_i K_i - \omega_i \sum_{j=1}^{N} \frac{D_i}{M} M_j K_j \tag{28}$$

where K_i is a thermal diffusion coefficient given by the relationship

$$K_i = -\frac{1}{P}\sum_{j=1}^{N}(\beta_{ij} - \beta_{ji}) \tag{29}$$

Here β_{ij} is approximated by the expression

$$\beta_{ij} = -P\frac{x_i x_j \mu_{ij} \tau_j}{4 m_j \gamma_j D_{ij}} \tag{30}$$

where

$$\gamma_i = \frac{m_i}{2kT} \tag{31}$$

and

$$\frac{1}{\tau_i} = 2\sum_{j=1}^{N} \frac{n_j \sigma_{ij}}{\sqrt{\pi \gamma_{ij}}} \tag{32}$$

In these relations, k is Boltzmann's constant, m_i is the mass of a single molecule of the i^{th} species, n_i is the number density of the i^{th} species and

$$\mu_{ij} = \frac{m_i m_j}{m_i + m_j} \tag{33}$$

$$\gamma_{ij} = \frac{\gamma_i \gamma_j}{\gamma_i + \gamma_j} \tag{34}$$

$$\sigma_{ij} = \frac{\pi}{4}\left(\sigma_i + \sigma_j\right)^2 \tag{35}$$

where σ_i is the molecular collision diameter of the i^{th} species (and σ_{ij} is the total cross-section for "i-j" collisions). Note that τ_i represents the mean time between collisions of molecules of the i^{th} species. The form of Eq. (30) differs from that given in Ref. 12, and was suggested by Ramshaw [8]. Finally, note that the form of Eq.. (28) guarantees that the sum of the thermal diffusion fluxes over all species is zero.

Reaction Models

In CVD applications two forms of reaction need to be modeled. The first type of reactions is homogeneous reactions in which the input gases react to form gas phase products. These reactions are described with classical gas phase reaction models. However, in CVD applications it is the deposition on the wafer surface that provides the desired end product. These surface reactions are less well documented than the gas phase reactions. Both types are now discussed.

Gas phase reaction model

The last term $\sum_{j=1}^{J} R_{i,j}$ in Eq. (4) represents the sum of the rate of production or consumption for the i^{th} species from each reaction j. The chemical equation (conservation of atoms) for the general elementary reaction j can be written as

$$\sum_{i=1}^{N} \nu'_{i,j} X_i \;\rightleftarrows\; \sum_{i=1}^{N} \nu''_{i,j} X_i \qquad (j = 1,J) \tag{36}$$

where $\nu'_{i,j}$ and $\nu''_{i,j}$ are the stoichiometric coefficients of the i^{th} species on the reactant and product sides, respectively, of reaction and X_i is the chemical symbol for the i^{th} species. In homogeneous reactions, the production rate is given by

$$R_{i,j} = M_i\left(\nu''_{i,j} - \nu'_{i,j}\right)\left[k_{f_j}\prod_{i=1}^{N}[X_i]^{\nu'_{i,j}} - k_{r_j}\prod_{i=1}^{N}[X_i]^{\nu''_{i,j}}\right] \qquad (37)$$

where k_{f_j} is forward reaction rate constant for reaction j which can normally be expressed in terms of the usual Arrhenius form, k_{r_j} is the rate constant for the reverse reaction, and $[X_i] = \rho_i / M_i$ is molar concentration of the i^{th} species. For reversible reactions, the reverse reaction rate constant, k_{r_j}, is related to the equilibrium constant K_c by $k_{r_j} = k_{f_j} / K_c$. The equilibrium rate constant can be computed from thermodynamic properties (Gibb's free energy) using standard procedures. Specific materials chemistry and reaction data to be considered in this work are discussed in a subsequent section.

Surface process model

The surface deposition models used in this study are similar to that described in ref. [9]. The heterogeneous reactions occurring at the interface between a solid substrate surface and a mixture of flowing gases, the fluid-substrate interface, leading to the deposition of bulk phase specie(s) can be viewed as a two step process. In the first step the gaseous molecules are diffused to the surface where some are adsorbed onto the various surface level sites. In this study the number of surface level sites is assumed to be a know quantity which is a function of the deposition surface. The second step consists of surface chemical reactions and deposition of products into the bulk phase. In general it is also possible to have desorption of bulk phase species to the surface level and of surface species to the gaseous state. It is clear from this discussion that a surface site is an active participant in this scheme. In the following discussion (g) represents a gas phase species, (s) denotes an adsorbed surface species on the top-most layer of the solid and (b) denotes a deposited solid. The notation and handling procedure for surface species and reactions can be done in a manner similar to the gas phase reactions. In analogy with Eq. (36), the surface reactions can be written

$$\sum_{i=1}^{K}\nu'_{i,j}X_i \;\underset{\leftarrow}{\rightarrow}\; \sum_{i=1}^{K}\nu''_{i,j}X_i \qquad (j = 1, J^s) \qquad (38)$$

where in this case K represents all the species regardless of phase (gaseous, surface and bulk), J^s is the total number of surface reactions and X_i is the chemical symbol of the i^{th} species. In general all N gaseous species are included in Eq. (38). The mass rate of deposition of the i^{th} species per unit area per unit time, $\dot{s}_i$, can be calculated from

$$\dot{s}_i = M_i \sum_{j=1}^{J^s} \left(\nu''_{i,j} - \nu'_{i,j} \right) q_j \qquad (i=1,K) \qquad (39)$$

where q_j represents the rate of progress variable for the j^{th} surface reaction. In this study several forms of q_j have been used.

The most general form for q_j uses a form similar to Eq. (37)

$$q_j = k_{f_j} \prod_{i=1}^{K} [X_i]^{\nu'_{i,j}} - k_{r_j} \prod_{i=1}^{K} [X_i]^{\nu''_{i,j}} \qquad (40)$$

where the same notation is used as that for Eq. (37) except that all variables are with respect to the surface reactions. For gaseous species at the surface, the concentration of the i^{th} species in moles / cm^3, $[X_i]$, is defined the same as for homogeneous chemistry. For the site species the concept of a site fraction, Z_i, is introduced. The site fraction for the i^{th} surface species, Z_i, is related to the concentration of the i^{th} surface species, [Xi], by

$$[X_i] = \frac{Z_i \Gamma}{\sigma_i} \qquad (i = N_s^f, \ldots\ldots, N_s^l) \qquad (41)$$

where Γ is the site density usually in moles / cm^2 and σ_i is number of sites occupied by the i^{th} species and where N_s^f is the first site species and N_s^l is the last site species. Note that the concentration of the surface (or site) species is also in moles / cm^2. By definition the sum of the site fractions over all surface species is equal to unity

$$\sum_{i=N_s^f}^{N_s^l} Z_i = 1 \qquad (42)$$

For bulk species, concentrations are defined in terms of the bulk species activities, α_i

$$[X_i] = \alpha_i \qquad (i = N_b^f, \ldots\ldots, N_b^l) \qquad (43)$$

where N_b^f is the first bulk species and N_b^l is the last bulk species. The activities are non-dimensional.

In this study we have limited ourselves to cases of only forward (irreversible) reactions with only gaseous and site species on the left hand side of Eq. (38). This eliminates the need for knowledge of reverse reaction rates and bulk species activities. All species, gaseous, site and bulk, can occur on the right hand side of Eq. (38). In the steady state the rate of production of site species from the gaseous species is equal to the rate of

production of the bulk species from the site species. Therefore, the net production of individual surface species is zero or

$$\dot{s}_i = 0 \qquad (i = N_s^f, \ldots\ldots, N_s^l) \tag{44}$$

Because there are no bulk species on the left hand side of Eq. (38), this results in a system of $N_s^l - N_s^f + 1$ (in general) nonlinear equations which can easily be solved by standard techniques. This method requires that the system of reactions defined by Eq. (38) have all site species on both the left and right hand side of at least one (not the same) reaction. If this were not the case the only solution would be a zero site fraction for that species. Once the system of equations represents by Eq. (44) is solved, the rate of depletion and production of the gaseous species and the rate of production of the bulk species can be calculated by the use of Eq. (39). As will be shown in the **Boundary Conditions** section, the surface reactions are strongly coupled to both the fluid flow as described by Eqs. (1) - (4) and the heat conduction equation in the solid surface.

In general the rate coefficients, k_{f_j} and k_{r_j}, in Eq. (40) can be written in the Arrhenius form

$$k_{f_j} = A_j T^{\beta_j} e^{-\frac{E_j}{RT}} \tag{45}$$

where A_j, β_j and E_j are known coefficients.

The sticking coefficient model is a subset of Eq. (45) where the relationship is

$$k_{f_j} = \nu_i \sqrt{\frac{RT}{2\pi M_i}} \tag{46}$$

where ν_I is the "sticking coefficient" for the i^{th} species in reaction j. Sticking coefficient approximations are commonly used in surface chemistry models. Although under some conditions the sticking coefficient model may give reasonable results, it is in general unreliable. For most cases the surface chemistry process is more complex than that which can be described by a sticking coefficient and hence has not been used in this study.

In some cases it is desirable to use models where k_{f_j} and k_{r_j} have a non-Arrhenius or modified Arrhenius form where the values of k_{f_j} and k_{r_j} can be functions of the concentration of the reacting species. In other cases the values of the q_j's are functions of the concentrations of one or more of the reacting species. In the results section the various models will be discussed as they are used.

Usually the desired end result of a calculation is the deposition rate, $\dot{r}$, in cm / sec of the bulk species on the substrate surface is given by

$$\dot{r} = \sum_{i=N_b^f}^{N_b^l} \frac{\dot{s}_i}{\rho_i} \tag{47}$$

where ρ_I is the density of the i^{th} bulk species and the mass flux to the surface in gm / cm^2 · sec, $\dot{m}$, is given by

$$\dot{m} = \sum_{N_b^f}^{N_b^l} \dot{s}_i \tag{48}$$

Transport and Thermodynamic Properties

For the deposition of a given material, the transport properties such as viscosity, thermal conductivity and diffusivity must be specified as a function of temperature and pressure. These are obtained from Lennard-Jones parameters for each of the chemical species [10,11]. Note that all physical properties vary across the reactor with a variation in temperature and composition; therefore assumption of constant properties is not appropriate. Thermodynamic properties such as heat capacity, enthalpy, entropy, and free energy for each species are obtained from the NASA Lewis database which has been added to the code to compliment the Sandia National Laboratory database. These databases contains data for many silane and chlorosilane species used in structural materials preparation.

Boundary Conditions

A complete problem definition requires specification of boundary conditions. At a subsonic inflow boundary, mass flux distribution, flow angles and total temperature are specified. This has proven very effective for a wide variety of cases. For species, Danckwert's boundary condition is used at the inlet. This condition equates the incoming species mass fluxes to the net convective and diffusive fluxes at the inlet. This is an alternative to specifying the mass or mole fractions at the inlet. However, if desired mass fractions may be specified. Outflow boundary conditions require setting downstream pressure and extrapolation of species densities, temperature and velocity.

At non-deposition walls, the no-slip condition is imposed for velocities. At the substrate and boundaries where deposition occurs, a mass balance for each species equates the flux to the growth surface and the net production of that species in surface reactions. In representing the surface reactions, one needs to include detailed mechanisms including adsorption and desorption kinetics, as discussed earlier [12]. This yields

$$\mathbf{n} \cdot (\mathbf{j}_i + \rho_i \mathbf{U}) = \dot{s}_i M_i \tag{49}$$

where again the subscript i refers to the i^{th} gaseous species and **n** refers to the unit normal vector. The term $\dot{s}_i$ represents the molar rate of deposition of species k at the interface. Note also that the net growth rate results in a non-zero mass-averaged normal velocity at the growth surface, viz.,

$$\mathbf{n}\cdot\rho\mathbf{U} = \sum_{i=1}^{N} \dot{s}_i M_i \tag{50}$$

Equation (50) can be derived by summing Eq. (49) over all gaseous species since the sum of all diffusional fluxes must be zero. When there is no surface deposition Eq. (49) reverts to the standard wall species boundary condition

$$\mathbf{n}\cdot\mathbf{j}_i = 0 \tag{51}$$

If the effects of pressure and thermal diffusion are neglected or negligible Eq. (51) becomes the simpler condition

$$\mathbf{n}\cdot\nabla\rho\omega_i = 0 \tag{52}$$

In addition when there is no surface deposition Eq. (50) becomes the no through flow condition

$$\mathbf{U} = 0 \tag{53}$$

For the thermal condition it is common to specify either the temperature or heat flux at the reactor wall (the adiabatic condition is a special case of specified heat transfer). If the heat flux is specified, it may be necessary to include both conduction and radiation effects. Inclusion of radiation heat transfer may be necessary because of the radiation heat exchange between heated susceptor, walls and windows. For the outer wall, a conductive description may be adequate. Although the specification of the heat flux or surface temperature is commonly used, it is well known that the substrate temperatures are not constant or the heat transfer rates are imprecisely known. A more general approach is to solve the heat conduction equation in the solid simultaneously with the fluid dynamic equations. In this case it is necessary to specify a compatibility condition at the between the fluid and the solid substrate.

When the heat conduction equation is solved in conjunction with the fluid mechanical equations (the so-called conjugate technique), the energy transfer within the solid material is governed by the heat conduction equation of the form

$$\rho_s C_{p_s} \frac{\partial T_s}{\partial t} = \nabla\cdot\kappa_s\nabla T_s + Q_s \tag{54}$$

where ρ_s C_{p_s} κ_s and T_s are the density, specific heat, thermal conductivity and temperature respectively of the solid. Q_s represents any non-conductive heat generation within the solid as for example might be due to inductive heating. The solid material properties do not have to be constant and are often represented as a functions of temperature. The compatibility condition at the interface of the fluid and the solid surface ensures that the temperature and the heat transfer across the interface are consistent. Therefore, at the interface junction, the temperature of the fluid and the solid must be the same

$$T_g = T_s \tag{55}$$

while the energy balance at the interface is given by

$$\mathbf{n}\cdot\kappa_g\nabla T_g - \sum_{i=1}^{K} \dot{s}_i M_i h_i(T) = Q_R + \mathbf{n}\cdot\kappa_s\nabla T_s \tag{56}$$

The terms on the left hand side of Eq. (56) represent the conductive heat transfer from the fluid and the heat transfer due to deposition. Species are summed over all K (gaseous, solid and bulk) species at the interface. The terms on the right hand side of the equation represent radiation, Q_R, and conductive heat transfer into the solid. In this equation the subscript g represents the gaseous (fluids) values at the interface. In practice the fluid dynamics equations and the heat conduction equation are solved independently with the above compatibility equations enforced as the boundary conditions.

When the conjugate problem is considered in this study, the solution procedure is to first solve the fluid dynamic equations with specified interface temperatures. The heat transfer rate from the fluids to the solid surface and the deposition energy transfer (the first and second terms of the left hand side of Eq. (56) are calculated and then imposed on the heat conduction equation as the boundary condition. The heat conduction is then solved, the surface temperatures calculated and imposed on the fluid dynamics. The overall process is repeated until both the fluid dynamic equations and the heat conduction equation are converged.

Solution and Numerical Procedure

General

The basic numerical procedure and in-house computational fluid dynamics code has been developed by SRA personnel over many years. The current capability includes two and three dimensional analysis, reacting flow, two phase flow and multiple turbulence models. More recently, as will be discussed subsequently, SRA under its own funds has developed an incompressible (or very low Mach number) capability in which pressure coefficient appears specifically as a dependent variable. Applications of the code, numerical procedure and grid capability have been made to a wide range of practical problems for DOD and NASA including turbo-machinery, primary and secondary gas

paths, re-entry vehicles, rocket motors, inlets, seals, chemical lasers, combustion, two and multi-phase flows, crystal growth and CVD. Examples can be found in [12-23].

Algorithm

The numerical algorithm which forms the basis for this code is described below. The procedure to solve the governing equations is a consistently split linearized block implicit scheme originally developed by Briley and McDonald [24] at SRA and embodied in a computer code termed MINT. The basic algorithm has been further developed and applied to both laminar and turbulent flows (see Briley and McDonald [25]). The method can be outlined as follows: the governing equations in a non-dimensional form are replaced by an implicit time difference approximation. Terms involving nonlinearities at the unknown time level are linearized by Taylor series expansion about the solution at the previous known time level, and spatial difference approximations are introduced. The result is a system of multi-dimensional coupled (but linear) difference equations for the dependent variables at the unknown or implicit time level. To solve these difference equations, the Douglas-Gunn procedure for generating alternating direction implicit (ADI) splitting schemes is used. This ADI splitting technique leads to systems of coupled linear difference equations having narrow block-banded matrix structures which can be solved efficiently by standard block-elimination methods.

Low Mach number or incompressible flow considerations

Very low Mach number or incompressible flow can lead to stability problems for the solution procedures described above. Basically at very low Mach numbers the solution matrix becomes ill-conditioned leading to slow or non-convergence and, perhaps, to loss of accuracy. The difficulties increase when significant temperature variation is present as is normally the case in CVD processes.

Under a corporate IR&D program, SRA has extended its Navier Stokes solution procedure to low Mach number or incompressible flows. With this approach density, ρ, is replaced by the pressure coefficient, c_p, as a dependent variable. The global continuity, momenta and species continuity governing partial differential equations, Eqs. (1) - (4), are recast in the form

$$\alpha \frac{\partial\left(\frac{\rho c_P}{2}\right)}{\partial t} + \nabla \cdot \rho \mathbf{U} = \mathbf{0} \tag{57}$$

$$\frac{\partial \rho \mathbf{U}}{\partial t} + \nabla \cdot \rho \mathbf{U}\mathbf{U} = -\frac{1}{2}\rho_\infty U_\infty^2 \nabla c_p + \nabla \cdot \boldsymbol{\tau} + \rho \mathbf{g} \tag{58}$$

$$\frac{\partial \rho h}{\partial t} + \nabla \cdot \rho h \mathbf{U} = -\nabla \cdot \mathbf{q} + \frac{1}{2}\rho_\infty U_\infty^2 \frac{Dc_P}{Dt} + \Phi + \mathbf{Q}_{ext} \tag{59}$$

and

$$\alpha\frac{\partial\left(\frac{\rho\omega_i c_p}{2}\right)}{\partial t}+\nabla\cdot\rho\omega_i\mathbf{U}=-\nabla\cdot\mathbf{j}_i+\sum_{j=1}^{J}R_{ij} \tag{60}$$

where α is an arbitrary constant and the pressure coefficient, c_p, is defined by

$$c_p=\frac{P-P_\infty}{\frac{1}{2}\rho_\infty U_\infty^2} \tag{61}$$

For solutions where only steady state is of interest the solution obtained from Eqs. (57) - (60) are the same as the solution obtained from Eqs. (1) - (4). The main advantage in solving this modified set of equations is that the dependent variable, c_p, does not have the large spatial variation that the density, ρ, has especially when there are large temperature gradients. Hence the convergence and stability characteristics of the governing equations are better behaved. When Eq. (5) is substituted into Eq. (61) a new form of the equation of state is obtained

$$\rho=\frac{M}{RT}\left(P_\infty+\frac{1}{2}\rho_\infty U_\infty^2 c_p\right) \tag{62}$$

Because of the artificial time terms in the global continuity and the species conservation equations the above equations cannot be used for time accurate solutions. Time accurate forms of Eqs. (1) - (4) can be obtained by augmenting the physical time derivatives with artificial time terms (as described above) of the form $\frac{\partial}{\partial\tau}$ where τ represents an artificial inner iteration time term chosen to accelerate inner convergence. For this case the governing equations take the form

$$\frac{\partial\rho}{\partial t}+\alpha\frac{\partial\left(\frac{\rho c_P}{2}\right)}{\partial\tau}+\nabla\cdot\rho\mathbf{U}=\mathbf{0} \tag{63}$$

$$\frac{\partial\rho\mathbf{U}}{\partial t}+\frac{\partial\rho\mathbf{U}}{\partial\tau}+\nabla\cdot\rho\mathbf{U}\mathbf{U}=-\frac{1}{2}\rho_\infty U_\infty^2\nabla c_p+\nabla\cdot\boldsymbol{\tau}+\rho\mathbf{g} \tag{64}$$

$$\frac{\partial\rho h}{\partial t}+\frac{\partial\rho h}{\partial\tau}+\nabla\cdot\rho h\mathbf{U}=-\nabla\cdot\mathbf{q}+\frac{1}{2}\rho_\infty U_\infty^2\frac{Dc_P}{Dt}+\Phi+\mathbf{Q}_{ext} \tag{65}$$

and

$$\frac{\partial \rho \omega_i}{\partial t} + \alpha \frac{\partial \left(\frac{\rho \omega_i c_p}{2} \right)}{\partial \tau} + \nabla \cdot \rho \omega_i \mathbf{U} = -\nabla \cdot \mathbf{j}_i + \sum_{j=1}^{J} \mathbf{R}_{ij} \tag{66}$$

Eqs. (63) - (66) are the same as Eqs. (1) - (4) if the artificial time terms are neglected. Time accurate solution of Eqs. (63) - (66) are obtained by using an inner iteration - outer iteration solution procedure. In the inner iteration procedure the time step τ is chosen to optimize inner convergence of the iteration procedure. The time accurate portion of the solution is determined from the physical time term.

•RESULTS

General

The analysis described above has been applied to a number of test cases. Although the physics, homogeneous and heterogeneous chemistries and geometries of the cases are significantly different, there are certain common features that apply to the general form of the input and output of all the cases. The cases have all been run with the MINT computer code which solves the Navier-Stokes equations in the gaseous flow and the heat conduction equation (if desired) in the solid substrate with the appropriate compatibility conditions and heterogeneous surface chemistry applied at the interface. The input for all cases is outlined in Table I. Input is divided into three parts: (1) Reactor Input, (2) Substrate Input and (3) Deposition Surface Input. The reactor and substrate geometries must be compatible, i.e., at the fluid-substrate interface the two geometries must be coincident. The grids do not have to match grid point to grid point. Interpolation procedures can be used to transfer information from the fluids grid to the substrate grid and vice versa. For all cases considered, the flow is subsonic with the Mach number being on the order of 10^{-3} to 10^{-4}. This requires the use of the subsonic inlet and exit boundary conditions described in the boundary conditions section and outlined in Table I. The homogeneous chemistry used will be described in detail for each case. In some cases the homogeneous chemistry involves many chemical species with numerous chemical reaction described by Arrhenius type reactions. In still other cases the homogeneous chemistry uses a "global" description where a semi-empirical formula is used to describe the homogeneous chemistry. In other cases there are no homogeneous reactions. All the reactions take place at the fluids-substrate interface in the form of heterogeneous reactions.

Substrate conditions are usually straight-forward. In the temperature range of interest the density, specific heat and thermal conductivity of the substrate material are normally considered to be known constants. Usually in CVD applications there is a desired target temperature at the fluids-substrate interface. In practice a thermocouple is embedded in the surface to approximately monitor this temperature and the amount of energy applied to the substrate is modified until that desired temperature is achieved. In the numerical simulation the surface temperature is either directly set (if the conjugate technique is not used) or the surface temperature is numerically monitored (if the conjugate technique is used) and the substrate backface boundary condition is modified until the desired temperature is achieved.

The input for the heterogeneous chemistry is similar to the homogeneous chemistry. Both Arrhenius and non-Arrhenius heterogeneous chemistries have been used as well as "global" techniques. When the Arrhenius site fraction techniques have been used the site or surface species deposition rates are determined from the equilibrium condition previously described. Therefore it is not necessary to know the surface species thermo-chemical properties necessary to calculate the species enthalpy in Eq. (56)

REACTOR INPUT

- Reactor Geometry
- Boundary Conditions
  - Input Flow Conditions
    - Mass Flux
    - Stagnation Temperature
    - Composition
  - Exit Conditions
    - Specified Static pressure
  - Symmetry Conditions
  - Wall or Surface Conditions
    - Deposition
    - Heat Transfer
- Homogeneous Rate Chemistry
- Gaseous Species Thermo-chemical Data

SUBSTRATE INPUT

- Substrate Geometry
- Material Properties
- Surface Boundary Conditions
  - Deposition
  - Symmetry
  - Heat Transfer Specified
  - Temperature Specified

DEPOSITION SURFACE INPUT

- Heterogeneous Rate Chemistry
- Surface and Bulk Species Thermo-chemical Data
- Site Density

Table I. CVD Reactor Input

The form of the output obtained for all cases is shown in Table II. In the reactor all flow variables, dependent as well as derived variables, are produced as part of the output and can be displayed, plotted or averaged as desired by the user. Species distribution can be displayed as mass fractions, mole fractions or concentrations. Flow

REACTOR OUTPUT

- Flow Patterns
- Temperature Field
- Pressure Field
- Species Distribution
- Other Variables

SUBSTRATE OUTPUT

- Temperature Field

DEPOSITION SURFACE OUTPUT

- Film Growth Rate
  - Removal of Gases
  - Deposition of Bulk Species
  - Growth Rate Uniformity
- Film Composition

Table II. CVD Reactor Output

patterns can be obtained to aid in the design of more efficient CVD systems. When the conjugate technique is used, the temperature distribution and heat transfer rates in the substrate can be displayed. The ultimate objective of the CVD analysis is to obtain information about the film deposition process. One can display film growth rates, uniformity and composition as a function of the position on the fluids-substrate interface.

Test Cases

A series of six test cases have been run in this study. These cases have been chosen for a variety of reasons. Some were chosen because of the need to obtain information about critical DOD CVD programs, while others were chosen to demonstrate the ability of the above-described technique to duplicate more academic experimental data. All cases were run to the steady state using Eqs. (57) - (60) as the governing partial differential equations. Two of the six case were run with the conjugate technique, duplicating the calculations performed for the same physical device when using the specified temperature interface condition, the non-conjugate mode. The presentation of each case consists of information presented in a similar format. This includes: (1) a schematic drawing and brief verbal description of the physical device, (2) a table that contains flow input information necessary to perform the numerical calculation (3) tables showing the homogeneous and heterogeneous chemical reactions and associated rate constants and (4) a verbal and graphical description of the results and what the results

demonstrate. When a large number of cases were run, as was the case for the first four test cases, this section is described in the written text.

Silane–Propane and Methyltrichlorosilane - Cases I – IV

The first four cases considered in this study use the same basic CVD reactor geometry. A schematic of the device is shown in Fig. 1. It represents a typical vertical CVD reactor employed in semiconductor processing.

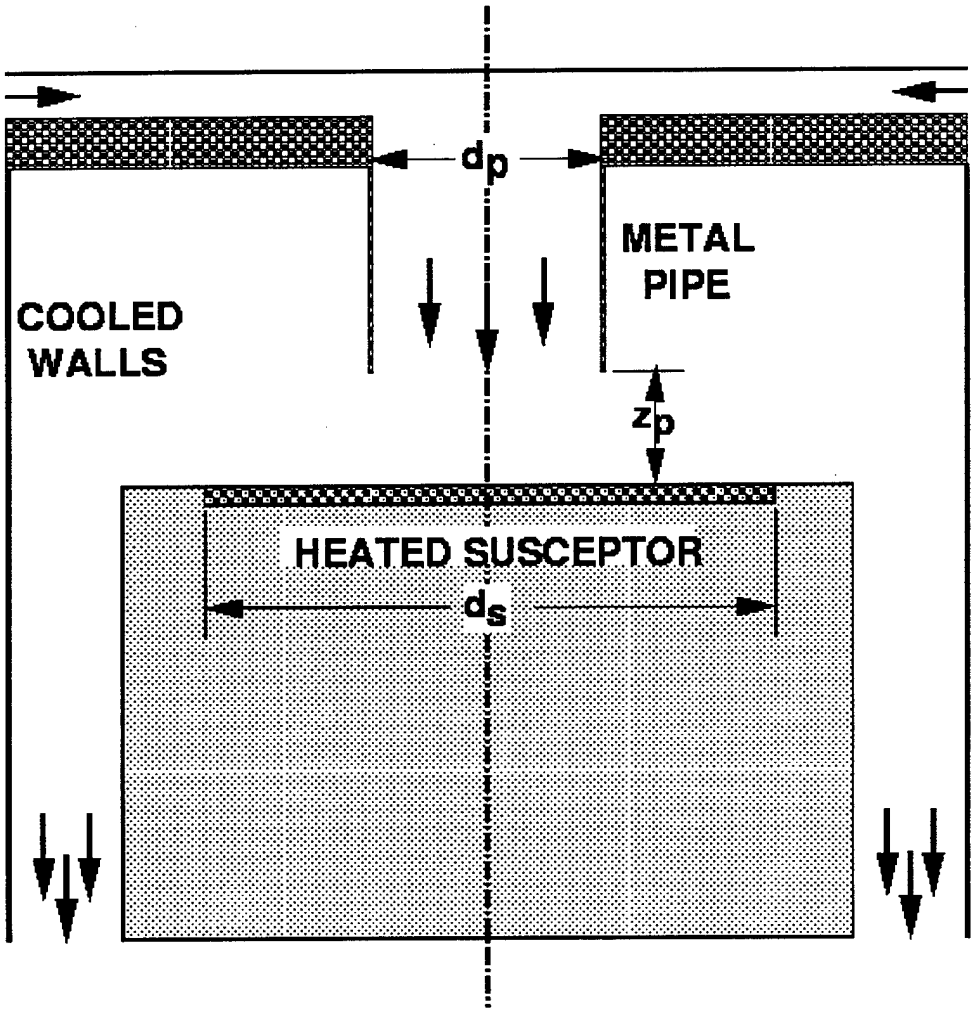

Fig. 1. Schematic Diagram for CVD Reactor

Flow containing the precursor gas and the carrier gas for SiC deposition enters from a surrounding inlet section on the top of the device, proceeds towards the centerline and is ducted down a metal pipe onto the heated susceptor where the deposition occurs. Flow then proceeds in a circuitous manner away from the centerline eventually exiting at the bottom of the device as shown. The reactor geometry is cylindrically symmetric and hence the computations are two-dimensional axisymmetric, i.e., the swirl component of

velocity is zero and there is no angular variation of any of the flow variables. Critical dimensions are noted on Fig. 1. d_p represents the diameter of the pipe, z_p represents the distance from the susceptor surface to the end of the pipe and d_s is the deposition surface diameter. Initially values of d_p and z_p were varied to determine 'optimum' values for deposition rate and consistency of thickness. These values were found to be 2 cm and 1 cm respectively. The value of d_s was always take as 5 cm. The temperature of the susceptor (substrate) was varied either directly (by specifying the susceptor temperature) or indirectly (by solution of the heat conduction equation in the susceptor and appropriate back face temperature) and the outer walls were assumed to be at room temperature. The inlet gas was at 290 K. For these cases, two feed precursor gases were considered: (1) Silane-Propane and (2) Methyltrichlorosilane (MTS). Both of the feed gases used hydrogen as a carrier gas. The molar ratio of the precursor gas to the hydrogen carrier gas considered were 10%, 20% and 40% with the majority of calculations performed at 10%. . The homogenous and heterogeneous reactions sets used in these calculations are shown in Tables III & IV for Silane-Propane and Tables V & VI for MTS. The homogenous Silane-Propane chemistry considered 13 individual species while the MTS homogenous chemistry considered 15 species. The heterogeneous Silane-Propane surface reactions require 8 additional chemical species while the corresponding MTS surface reactions require 7 additional species. Thus the Silane-Propane cases required the solution of 17 coupled partial differential equations and the MTS case required the solution of 19 coupled partial differential equations. The finite difference grid used for the computations consisted of 58 grid points in the axial direction and 45 grid points in the radial direction. Critical regions, such as the substrate and wall regions, used a concentration of grid cells in these regions relative to other places, the basic philosophy being that a dense concentration of cells is used where gradients are large.

When one considers the design of a CVD device many factors must be considered. First goodness criteria must be established by which you can evaluate the desired physical results. For this case two arbitrary criteria were used. The first is the deposition rate (usually measured in nm/min). The second is the uniformity of the deposition rate. Large growth rates are considered to be desirable while a large radial variation was considered to be undesirable and a more uniform variation was considered to be more desirable. Design parameters that one would consider certainly would include at least the following: (1) the mixture ratio of delivery precursor gas to carrier gas, (2) the total flow rate of precursor and carrier gas, (3) the delivery pressure of the gas and (4) the temperature of the susceptor surface. Also one could consider the above-mentioned dimensions of the CVD device. If all these possibilities were taken into consideration the matrix of possibilities would require a very large number of runs; therefore some compromise needed to be made. The technique used was to consider the geometry as frozen and to choose flow rate, pressure and susceptor pressure at set values (it will later be shown that these were not exactly arbitrary values). The values chosen for total volumetric flux of precursor and carrier gas was set as 600 standard cubic centimeters per minute (sccm). The notation sccm refers to the amount of volumetric flow rate that would correspond to the mass flux that occur at reference conditions of 1 atmosphere and room temperature. The pressure was chosen as 15.2 torr and the temperature of the susceptor was chosen as 1300 K. The

Reactions									A_j	β_j	E_j
1)	2H	+	M	⇔	H_2	+	M		$2.95x10^{18}$	-1.0	0
2)	CH_4	+	H	⇔	CH_3	+	H_2		$1.259x10^{14}$	0.0	11900
3)	CH_4	+	M	⇔	CH_3	+	H	+ M	$1.413x10^{17}$	0.0	88400
4)	$2CH_3$			⇔	C_2H_6				$8.913x10^{12}$	0.0	0
5)	C_2H_6	+	H	⇔	C_2H_5	+	H_2		$5.40x10^{2}$	3.5	5210
6)	C_2H_5	+	M	⇔	C_2H_4	+	H	+ M	$1.99x10^{15}$	0.0	30000
7)	$2CH_3$			⇔	C_2H_5	+	H		$2.80x10^{13}$	0.0	13592
8)	C_2H_6	+	CH_3	⇔	C_2H_5	+	CH_4		$5.50x10^{1}$	4.0	8300
9)	C_2H_4	+	H	⇔	C_2H_5				$2.21x10^{13}$	0.0	2066
10)	C_2H_4	+	M	⇔	C_2H_2	+	H_2	+ M	$1.50x10^{15}$	0.0	55800
11)	C_3H_8			⇔	C_2H_5	+	CH_3		$1.70x10^{16}$	0.0	84840
12)	SiH_4			⇔	SiH_2	+	H_2		$6.67x10^{29}$	-4.795	63450
13)	SiH_4			⇔	SiH_3	+	H		$3.69x10^{15}$	0.0	93000
14)	SiH_4	+	H	⇔	SiH_3	+	H_2		$1.46x10^{13}$	0.0	2500
15)	SiH_2	+	H	⇔	SiH	+	H_2		$1.39x10^{13}$	0.0	2000
16)	SiH_2	+	H	⇔	SiH_3				$3.81x10^{13}$	0.0	2000
17)	SiH	+	H_2	⇔	SiH_3				$3.45x10^{13}$	0.0	2000

Table III. Homogeneous Reactions: SiH_4 – C_3H_8 - H_2 System

Reactions										A_j	β_j	E_j
1)	CH_3	+	Si(s)	⇒	H_2	+	CH(s)	+	Si(b)	$8.67x10^{11}$	0.5	0
2)	CH_4	+	Si(s)	⇒	$2H_2$	+	C(s)	+	Si(b)	$4.20x10^{7}$	0.5	0
3)	C_2H_5	+	2Si(s)	⇒	$2H_2$	+	C(s)	+	CH(s) + 2Si(b)	$5.76x10^{20}$	0.5	0
4)	C_2H_4	+	2Si(s)	⇒	$2H_2$	+	2C(s)	+	2Si(b)	$9.37x10^{17}$	0.5	0
5)	C_2H_2	+	2Si(s)	⇒	H_2	+	2C(s)	+	2Si(b)	$1.22x10^{19}$	0.5	0
6)			2CH(s)	⇒	H_2	+	2C(s)			$2.25x10^{24}$	0.0	61000
7)	SiH_2	+	C(s)	⇒			SiH_2(s)	+	C(b)	$6.12x10^{11}$	0.5	0
8)	SiH_4	+	C(s)	⇒	H_2	+	SiH_2(s)	+	C(b)	$3.18x10^{10}$	0.5	18678
9)	SiH_3	+	C(s)	⇒	H_2	+	SiH(s)	+	C(b)	$6.03x10^{11}$	0.5	0
10)	SiH	+	C(s)	⇒			SiH(s)	+	C(b)	$6.23x10^{11}$	0.5	0
11)			2SiH(s)	⇒	H_2	+	2Si (s)			$2.25x10^{24}$	0.0	61000
12)			SiH_2(s)	⇒	H_2	+	Si (s)			$2.91x10^{14}$	0.0	9000

Table IV. Heterogeneous Reactions: SiH_4 - C_3H_8 - H_2 System

first variable to be investigated was the molar ratio of precursor gas to carrier gas for Silane-Propane. Three molar ratios of 10%, 20% and 40% were considered. Fig. 2 shows the results. As can be seen in Fig. 2, the radius varies from –2.5 cm to 2.5 cm or a total distance of d_s = 5.0 cm. The deposition rate is inversely proportional to the molar ratio. Also the uniformity of deposition remains relatively constant with respect to radius with some slight variation at a ratio of 10%. Therefore using our above criteria of goodness, it was decided to use a molar ratio of 10% for all subsequent investigations. It is recognized that this decision has a certain amount of arbitrariness and one might even make an argument for a molar ratio of 0.2 based on a slightly more uniform deposition.

Reactions									A_j	β_j	E_j
1)	2H	+	M	$\Leftrightarrow$	H_2	+	M		2.95×10^{18}	-1.0	0
2)	CH_4	+	H	$\Leftrightarrow$	CH_3	+	H_2		1.259×10^{14}	0.0	11900
3)	CH_4	+	M	$\Leftrightarrow$	CH_3	+	H	+ M	1.413×10^{17}	0.0	88400
4)	$2CH_3$			$\Leftrightarrow$	C_2H_6				8.913×10^{12}	0.0	0
5)	C_2H_6	+	H	$\Leftrightarrow$	C_2H_5	+	H_2		5.40×10^{2}	3.5	5210
6)	C_2H_5	+	M	$\Leftrightarrow$	C_2H_4	+	H	+ M	1.99×10^{15}	0.0	30000
7)	$2CH_3$			$\Leftrightarrow$	C_2H_5	+	H		2.80×10^{13}	0.0	13592
8)	C_2H_6	+	CH_3	$\Leftrightarrow$	C_2H_5	+	CH_4		5.50×10^{1}	4.0	8300
9)	C_2H_4	+	H	$\Leftrightarrow$	C_2H_5				2.21×10^{13}	0.0	2066
10)	C_2H_4	+	M	$\Leftrightarrow$	C_2H_2	+	H_2	+ M	1.50×10^{15}	0.0	55800
11)	$Si(CH_3)Cl_3$			$\Leftrightarrow$	$SiCl_3$	+	CH_3		7.60×10^{14}	0.0	69312
12)	$SiHCl_3$	+	H	$\Leftrightarrow$	$SiCl_3$	+	H_2		2.47×10^{12}	0.0	2543
13)	$SiHCl_3H$			$\Leftrightarrow$	$SiCl_2$	+	HCl		2.60×10^{11}	0.0	47000
14)	$SiCl_4$	+	H	$\Leftrightarrow$	$SiCl_3$	+	HCl		1.50×10^{12}	0.0	3400

Table V. Homogeneous Reactions: MTS - H_2 System

Reactions											A_j	β_j	E_j
1)	CH_3	+	Si(s)	$\Rightarrow$	H_2	+	CH(s)	+	Si(b)		8.67×10^{11}	0.5	0
2)	CH_4	+	Si(s)	$\Rightarrow$	$2H_2$	+	C(s)	+	Si(b)		4.20×10^{7}	0.5	0
3)	C_2H_5	+	2Si(s)	$\Rightarrow$	$2H_2$	+	C(s)	+	CH(s)	+ 2Si(b)	5.76×10^{20}	0.5	0
4)	C_2H_4	+	2Si(s)	$\Rightarrow$	$2H_2$	+	2C(s)	+	2Si(b)		9.37×10^{17}	0.5	0
5)	C_2H_2	+	2Si(s)	$\Rightarrow$	H_2	+	2C(s)	+	2Si(b)		1.22×10^{19}	0.5	0
6)			2CH(s)	$\Rightarrow$	H_2	+	2C(s)				2.25×10^{24}	0.0	61000
7)	$SiCl_2$	+	C(s)	$\Rightarrow$			$SiCl_2$(s)	+	C(b)		3.38×10^{11}	0.5	0
8)	H_2	+	$SiCl_2$(s)	$\Rightarrow$	2HCl	+	Si(s)				6.22×10^{4}	1.0	0
9)	$SiCl_3$	+	C(s)	$\Rightarrow$			$SiCl_3$(s)	+	C(b)		2.90×10^{11}	0.5	0
10)	H	+	$SiCl_3$(s)	$\Rightarrow$	HCl	+	$SiCl_2$(s)				6.22×10^{7}	1.0	0

Table VI. Heterogeneous Reactions: MTS - H_2 System

The second variable considered was the overall flow rate for both Silane-propane and MTS. The results are shown in Figs. 3-4 respectively. In both cases it can clearly be seen that 600 sccm is the best flow rate. It should also be noted that if a different geometric configuration had been chosen the results might have been different (not having performed those calculations this cannot be said with a complete degree of certainty).

The third variable considered was the pressure. Three pressures, 15.2 torr, 38.0 torr and 76.0 torr were chosen as representative of CVD applications. Figs. 5-6 show the results for injector pressures of Silane-Propane and MTS respectively. It is clearly seen that at 76.0 torr there is a large radial variation of growth rate. For both cases at 15.2 torr the growth rate is relatively uniform. As can be seen at 38.0 torr the variation in growth rate is only slightly less uniform than at 15.2 torr. However, a pressure of 15.2 torr was chosen as the reference condition for the remainder of this study.

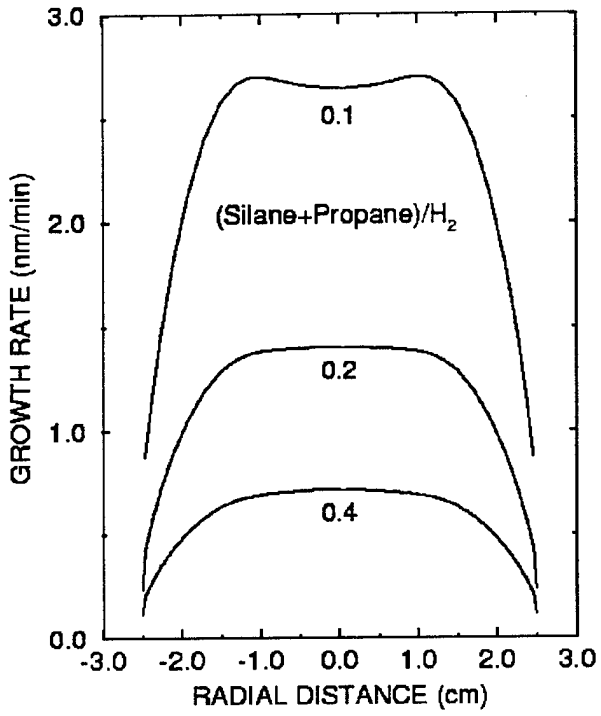

Fig 2. Silane-Propane Growth Rate vs. Radial Distance as a Function of Molar Ratio

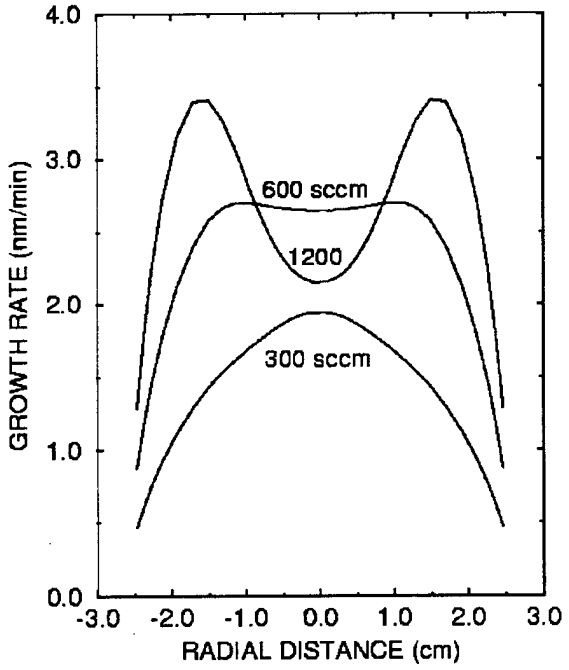

Fig 3. Silane-Propane Growth Rate vs. Radial Distance as a Function of Volumetric Flow Rate

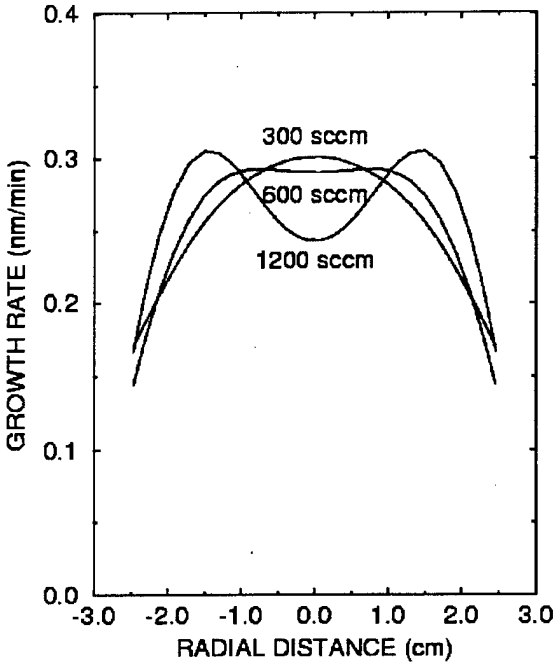

Fig 4. MTS Growth Rate vs. Radial Distance as a Function of Volumetric Flow Rate

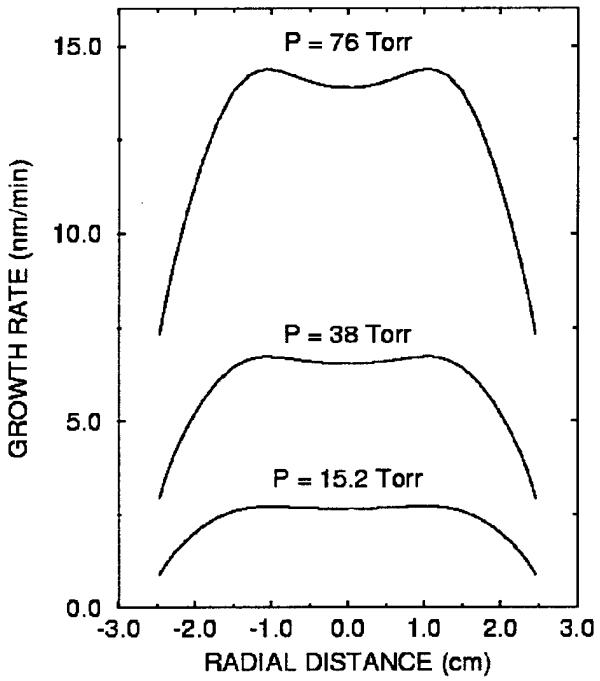

Fig. 5. Silane-Propane Growth Rate vs. Radial Distance as a Function of Inlet Pressure

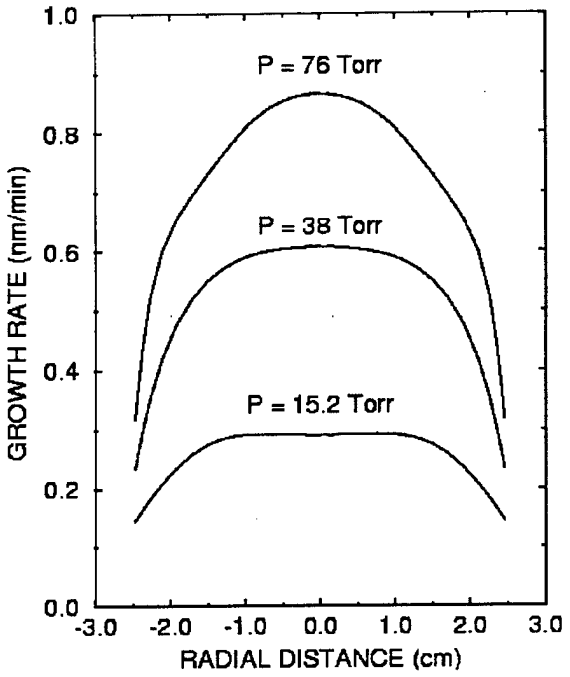

Fig. 6. MTS Growth Rate vs. Radial Distance as a Function of Inlet Pressure

The fourth variable considered was the susceptor temperature shown in Figs. 7-8.

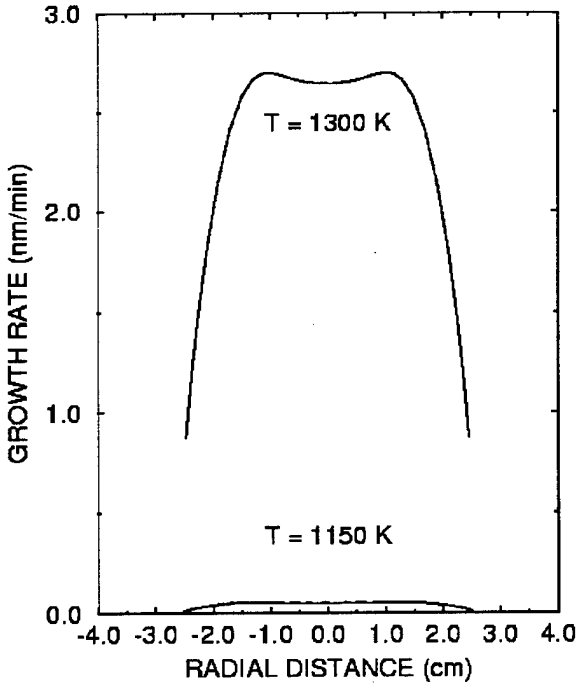

Fig. 7. Silane-Propane Growth Rate vs. Radial Distance as a Function of Susceptor Temperature

Three temperatures were chosen for the Silane-Propane case, 1300 K, 1450 K and 1600 K and three separate temperatures were chosen for the MTS case, 1000 K, 1150 K and 1300 K. These temperatures were chosen to be representative of CVD applications. For the Silane-Propane case, the 1000 K case yielded a value too small to appear on the figure. Even the 1150 K case yields a small deposition rate. The 1300 K case yields a significantly larger deposition rate with a fairly uniform radial variation. For the MTS case it is clear that the 1300 K case yields the most uniform deposition. At 1450 K and 1600 K the radial variation has no region of constant deposition rate.

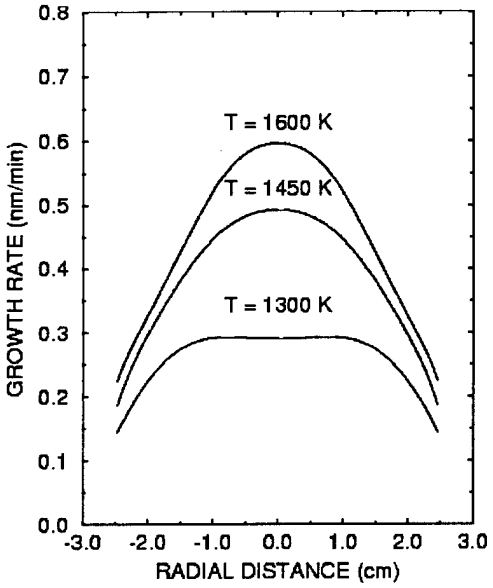

Fig. 8. MTS Growth Rate vs. Radial Distance as a Function of Susceptor Temperature

To test the conjugate capability two test cases were run, one with a Silane–Propane precursor and one with an MTS precursor. Both cases were run at the above derived 'optimum' or reference conditions of 600 sccm of precursor and carrier gas, 10% precursor gas, at an inlet pressure of 15.2 torr and a nominal susceptor temperature of 1300 K. The susceptor temperature was set indirectly by setting the backface temperature of the substrate at a nominal temperature. A converged solution was obtained and the average susceptor temperature calculated. Modifications were then made to the backface temperature until the desired or target susceptor temperature was obtained. This can be viewed as a simulation of a resistance-heating coil placed on the back of the substrate pedestal. One could then vary the current until the desired susceptor temperature was obtained. The geometry is the same as shown in Fig. 1. The substrate was assumed to be made from stainless steel with a specific gravity of 7.9, a specific heat of 594.4 joules / kg-K, and a thermal conductivity of 16.3 joules / m-sec-K. For the Silane-Propane case the backface of the substrate was set to 2378 K and for the MTS case the backface of the substrate was set to 2320 K. In both cases this led to a temperature of approximately

1300 K on the susceptor/fluids interface. To allow for a smooth variation of temperature at the lower left and right sides of the substrate, the temperature in these regions was smoothly lowered to 290 K over the last 0.84 cm of the substrate. Fig. 9 shows the temperature contours for both cases. This figure shows only the right-hand-side of the device portrayed in Fig. 1. The substrate is outlined with a black box in the lower left-hand-side of both cases. The 0.84 cm region where the backface temperature is lowered to 290 K is evident in this figure. It is important to note the continuity of temperature across all substrate/fluid boundaries, the so-call compatibility condition. Not only the temperature but also the heat transfer is continuous across these boundaries. While it is hard to discern from the figure, the heat transfer across the MTS/substrate boundary is slightly larger than for the comparable Silane-Propane case. This is probably due to the difference in the thermal conditions of the precursor gases. As might be expected the deposition rates were virtually the same as for the non-conjugate runs

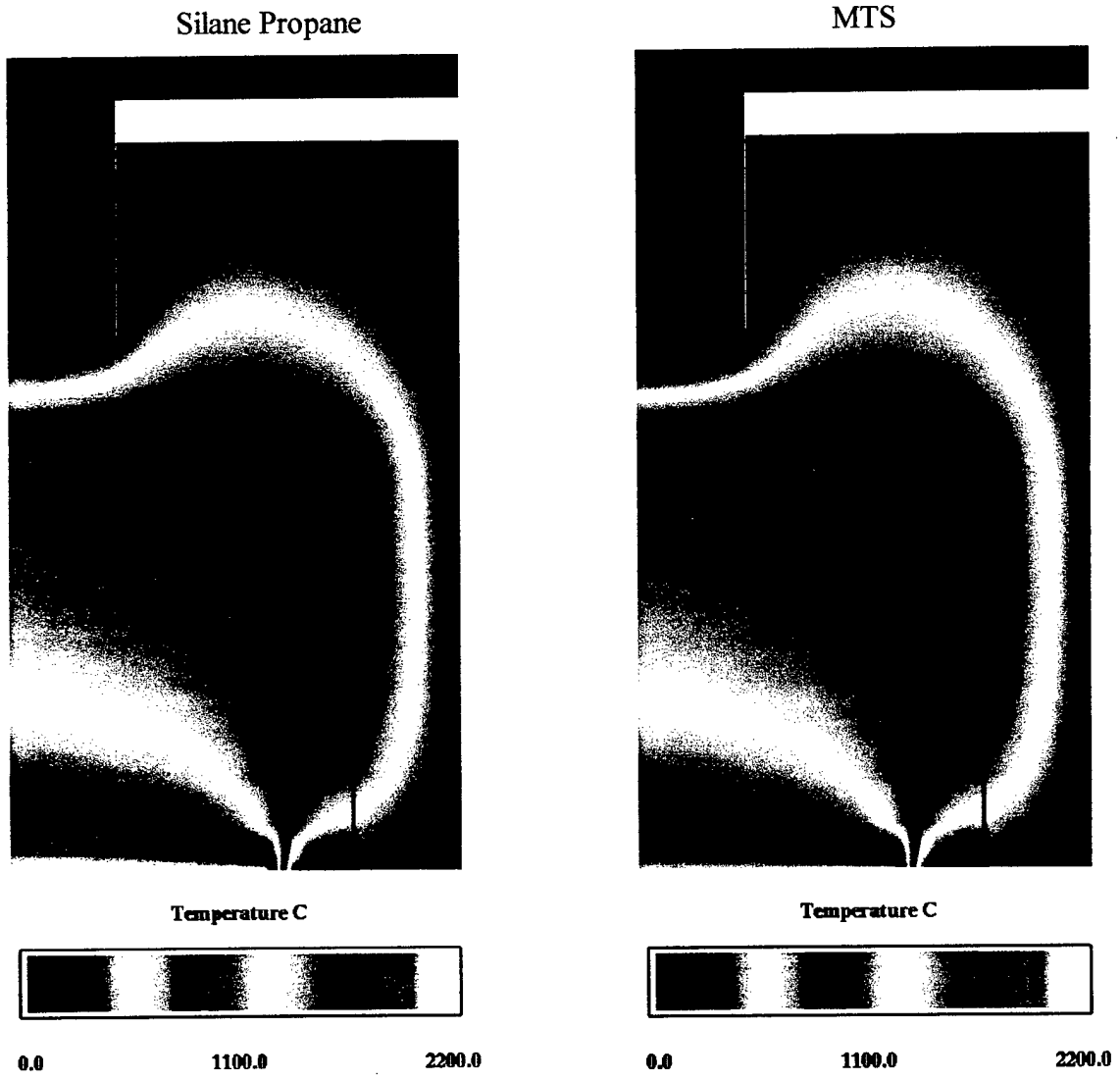

Figure 9. Temperature Contours for Silane-Propane and MTS at Standard Conditions

The purpose of the above exercise was to demonstrate the ability of the analysis to help the engineer to design a CVD device that can in some sense be optimized for a given set of parameters. Although the above did not survey all possible geometric designs or flow conditions, it does demonstrate the ability of the analysis to perform this task. In an actual design environment the experience of the designer would be used to get a preliminary design. Then a series of cases could be run in a manner similar to the above, but with an expanded matrix of possibilities, to achieve a desirable final design. The use of the conjugate heat transfer code coupled with the Navier-Stokes solver demonstrates an ability to solve the more complex problem where a surface temperature might not be known beforehand. In many cases the surface temperature is not know or is not a constant value and can only be determined in this manner.

Morton Cases I – III

A series of three test cases were run on a cylindrical device used by Morton International to deposit SiC. A schematic of the device is shown in Fig. 10. Flow enters from the top through the small injector and flows into the large cavity, through a nominal throat, impinges onto a disc, flows over the disc and exits through the bottom. The injector has a diameter of 0.305 in. and is 15 in. long. The cavity's diameter is 23 in. and has a length of 23 ¾ in. The nominal throat for the three cases is 5,8 and 10 in. and has a thickness of ¼ in. The case shown in Fig. 10 is for the 8 in. throat. The disc always has a diameter of 24 ¾ in. and a thickness of ¼ in. The diameter of the cavity containing the disc is 28 ¾ in. and has a length of 5 in. The exit pipe has a diameter of 4 in. with a length of 5 in. The overall length of the device is 49 in. All dimensions are to scale. The inlet injector, the leading edge of the first cavity, the trailing edge of the second cavity, the disc and exit pipe are assumed to be adiabatic. All other solid surfaces are heated to 1623 K. Deposition of SiC also occurs on all the heated walls as well as the disc. Flow conditions are the same for all three cases (the only difference is the throat diameter) and are presented in Table VII. The precursor gas is MTS while the carrier gas is a combination of hydrogen and argon at the rates shown in the table. In the table slm stands for standard liters per min, i.e., 1000 sccm. Because of the size of the device the flow was assumed to be turbulent. A turbulent k-ε turbulence model was used. This resulted in the solution of two additional partial differential equations, one for each of the variables. The homogenous and heterogeneous chemistry models are shown in Table VIII. This formulation was obtained from Morton International. The heterogeneous chemistry use a global model where the rate term is not of the standard Arrhenius form.

The region of primary interest in this study is the outer radius of the first, 23 in., cavity. Three computations were made using the non-conjugate computer program corresponding to the three different throat diameters. In each case 95 grid points were used in the radial direction and 120 grid points were used in the axial direction. As before grid points were packed in region where large gradients of flow variables were expected. Streamlines and temperature contours are shown in Fig. 11 for the 8 in. diameter throat

case, the left-hand-side showing the streamlines and the right-hand side showing the temperature contours. The streamlines show two large recirculation zones in the first

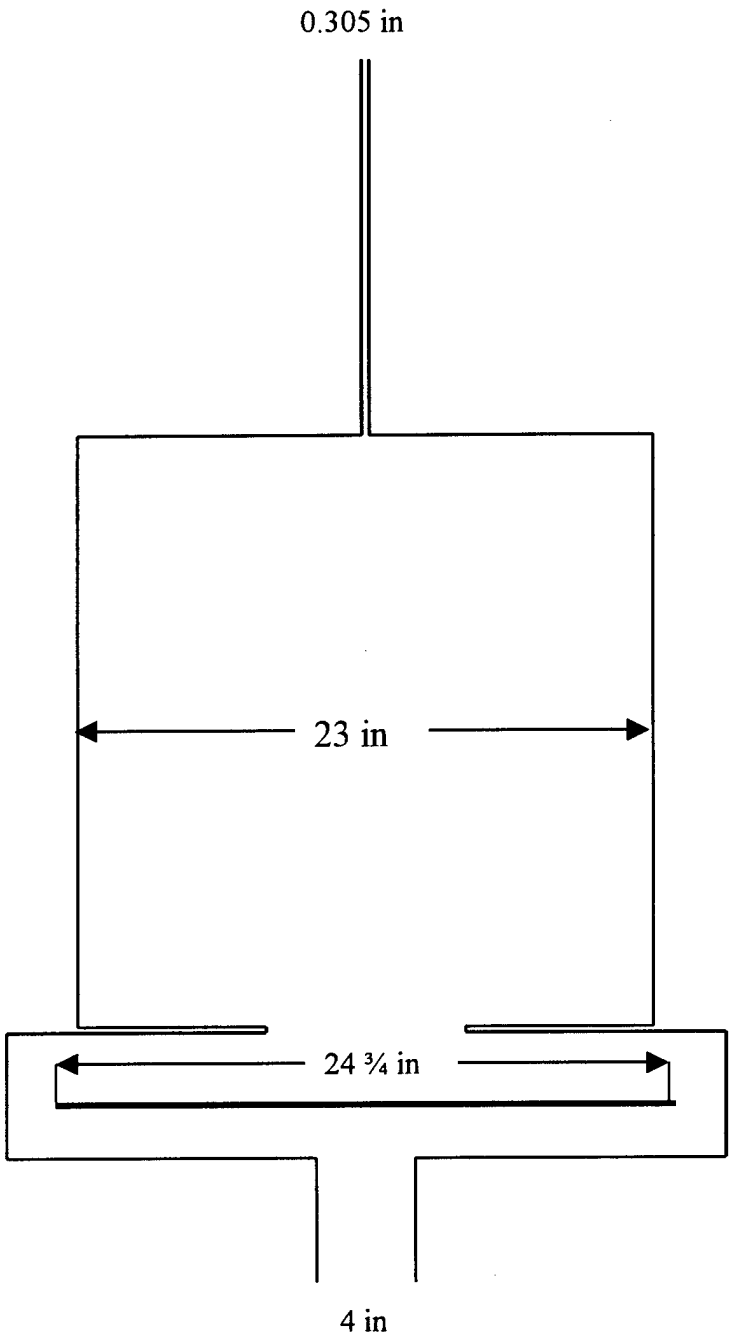

Figure 10. Schematic of Morton International Device

cavity. The recirculation zone nearest to the centerline rotates counter-clockwise while the one above it rotates clockwise. In can be seen that the recirculation zone nearest the centerline extends into the second cavity. Basically the flow exiting from the injector squirts along the centerline, up the face of the disc, over the top and down and out

through the exit pipe. This flow is only slightly heated by the outer walls. In looking at the temperature contours white is the hottest and blue the coldest, i.e., the temperature of the fluid entering the injector. The large clockwise recirculation zone adjacent to the outer wall of the first cavity is replenished by this primary flow with unreacted MTS. Since flow cannot be convected across streamlines, this process occurs by diffusion. The MTS then reacts in the high temperature regions near the heated walls and SiC is deposited on the walls. See Fig. 11.

Fig. 12 shows the growth rate on the outer wall of the first cavity as a function of the throat diameter. The 8in. and 10 in. diameter throats yield growth rates that are much more uniform than the 5 in. diameter throat case. By comparing the streamlines of the 8 in. diameter throat in Fig 11 with the streamlines for the 5 in. diameter throat in Fig 13 it is easy to see why that may be the case. While the 8 in. diameter throat case has two distinctive recirculation the 5 in diameter throat case has only one primary recirculation zone. In fact the single recirculation zone is much more intense in the region of the lower left corner of the first cavity. This probably leads to a much larger growth rate in this region as is seen in Fig. 12. The second recirculation zone in the 8in and 10 in diameter throat cases is moving much slower than the single recirculation zone in the 5 in. diameter throat case and is actually going in the opposite direction. The direction of the flow adjacent to the surface may account for the larger growth rates for the 8in. and 10 in. cases at the upper right-hand-side of the first cavity as is seen in Fig. 11 In all cases the uniformity of the growth rate is less than that observes in the calculations for cases I-IV above. This is probably due to the size and design of the device. Remember in Cases I-IV the device was somewhat sized and flow conditions modified to obtain a relative uniform deposition. No attempt was made to do that in this case. Instead the design and flow condition was taken as given by the manufacturer.

Morton Case I-III

Species	Flow Rate (slm)
MTS	7
H_2	41
Ar	33

Variable	Value
P_∞	200 torr
T_∞	290 K
Re / l_∞	26572 / cm
M_∞	0.409
T_{wall}	1623 K

Table VII. Flow Conditions – Morton Cases

Homogeneous Chemistry - Global Model

$$CH_3SiCl_3 + H_2 \underset{k_b}{\overset{k_f}{\rightleftarrows}} SiCl_2 + CH_4 + HCl$$

where the forward and backward rates are given by

$$k_f = A_f e^{-\frac{E_f}{RT}} \quad \text{and} \quad k_b = A_b e^{-\frac{E_b}{RT}}$$

where

$$A_f = 2.0 \times 10^{25} \ \frac{cm^3}{mole \cdot s} \qquad E_f = 1.07 \times 10^5 \ \frac{cal}{mole}$$

$$A_b = 1.1 \times 10^{32} \ \frac{cm^6}{mole^2 \cdot s} \qquad E_b = 9.95 \times 10^4 \ \frac{cal}{mole}$$

Heterogeneous Chemistry - Global Model

$$SiCl_2 + CH_4 \xrightarrow{k_f} H_2 + 2HCl + SiC(s)$$

where

$$k_f = \frac{A_f e^{-\frac{E_f}{RT}}}{\left(1 + k_a\left[X_{SiCl_2}\right] + k_b\left[X_{CH_4}\right]\right)^2}$$

and

$$k_a = A_a e^{-\frac{E_a}{RT}} \quad \text{and} \quad k_b = A_b e^{-\frac{E_b}{RT}}$$

where

$$A_f = 1.63 \times 10^{26} \ \frac{cm^4}{mole \cdot s} \qquad E_f = 7.64 \times 10^4 \ \frac{cal}{mole}$$

$$A_a = 5.00 \times 10^{10} \ \frac{cm^3}{mole} \qquad E_a = 5.16 \times 10^3 \ \frac{cal}{mole}$$

$$A_b = 7.11 \times 10^9 \ \frac{cm^3}{mole} \qquad E_b = 7.91 \times 10^3 \ \frac{cal}{mole}$$

Table VIII. Homogeneous and Heterogeneous Chemistry

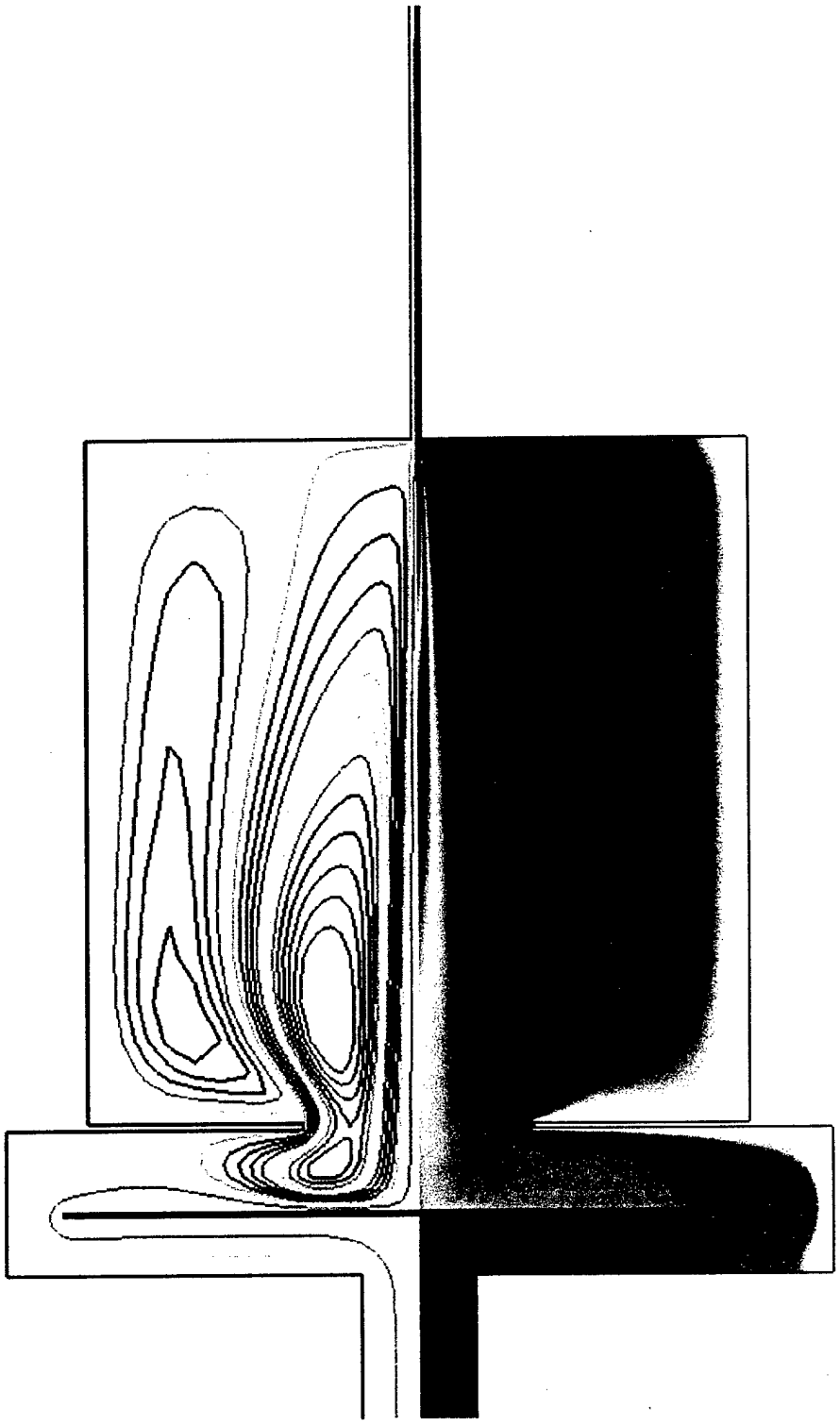

Figure 11. Morton Case 8 in Throat Streamlines and Temperature Contours

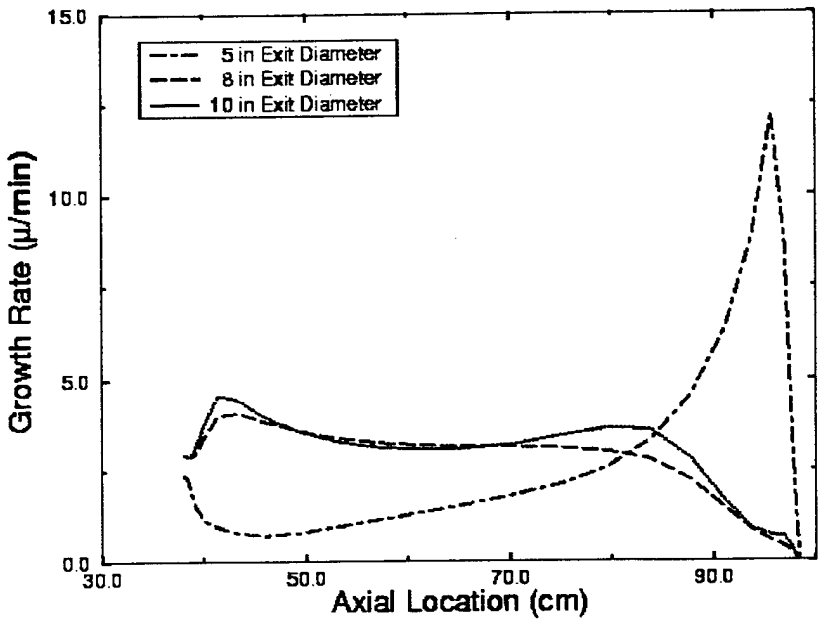

Figure 12. Morton Case Growth Rate versus Throat Diameter

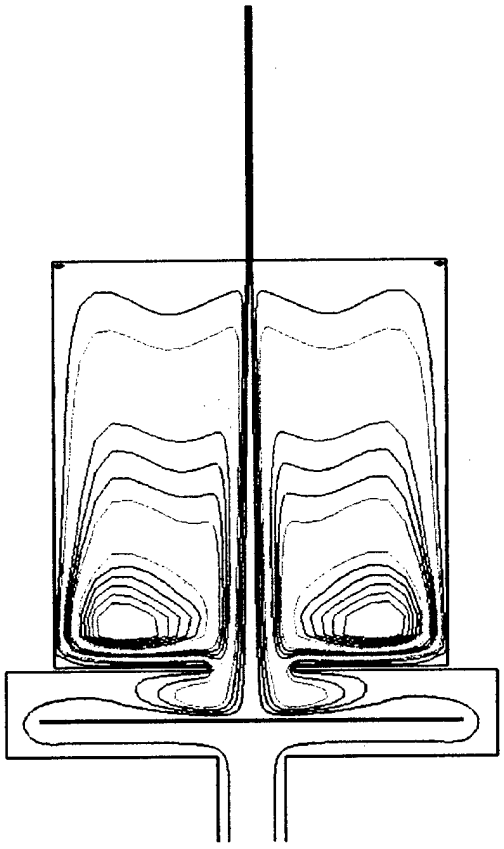

Figure 13. Morton Case 5 in Diameter Throat Streamlines

Papasouliotis and Sotirchos Cases

The last case considered was the experimental device of Papasouliotis and Sotirchos [26]. A schematic of the device is shown in Fig. 14. The schematic is expanded in the radial direction by a factor of 10 to emphasize the substrate. The white rectangle in the center is the substrate. As with the other cases considered the flow was considered to be axisymmetric. The diameter of the shroud/inlet section is 1.5 cm. Flow enters from the top of the device and passes over the graphite substrate. The substrate is 1.4 cm long and has a diameter of 0.191 cm. The substrate is hung from a digital microbalance that monitors the weight of the substrate as a function of time. Overall rates of deposition are obtained by differentiating the weight with respect to time. The outer walls that shroud the substrate are heated to a desired temperature profile. A region approximately 23 cm in length is heated to the target temperature. Both above and below this heating zone the temperature rapidly falls off to the temperature of the inlet gas. The temperature was monitored /measured by a series of thermocouples embedded in the shroud wall. Data were taken at a series of average shroud temperatures, inlet pressures, mass flux rates and substrate location. The substrate location refers to the distance of the midpoint of the substrate from the beginning or top of the heating zone. In this study three cases were considered; the flow conditions are shown in Table IX. All cases considered had a total flow rate of 200 sccm. The precursor gas is MTS and the carrier gas is hydrogen. The mixture ratio is 10%. The midpoint of the substrate was always 1.8 cm from the top of the heating zone. Calculations were performed with 30 radial grid points and 60 axial grid points. The overall length of the computational domain was 53 cm. The homogeneous and heterogeneous chemistry was the same as was used for previous MTS cases (see Tables III & IV).

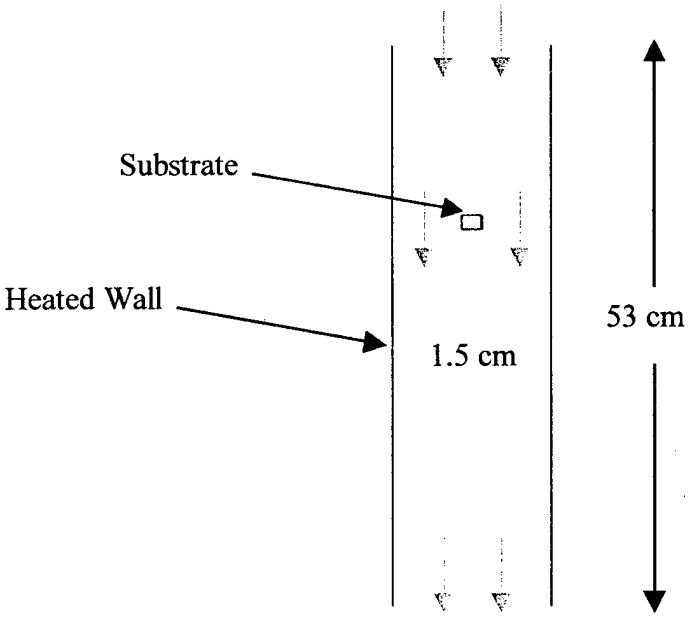

Figure 14. Schematic of Papasouliotis and Sotirchos Device

Comparison of the computational results with the experimental data is presented in Table X. In general the results are moderately encouraging at least with respect to the overall deposition rates. At the higher temperatures the comparison with date is relatively good. However at lower temperatures the predicted deposition rate continues to rise which is in contradiction with the data. Fig. 15 shows the temperature contours for the 900 C case. Because the device is so narrow the radial direction is expanded by a factor of 10. From this figure one can easily see the heat section of the shroud. It is also easy to see that the temperature (but not other flow variables) are essentially one-dimensional above and below the substrate. Moderate two-dimensional temperature effect can be seen in the region of the substrate.

Papasouliotis and Sotirchos Cases I-III

Species	Flow Rate (sccm)
MTS	18.18
H_2	181.82
Total	200.00

Variable	Value
P_∞	100 torr
T_∞	400 K
Re / l_∞	9.41 / cm
M_∞	0.000398
T_{wall} (Case I)	900 °C
T_{wall} (Case II)	1000 °C
T_{wall} (Case III)	1075 °C

Table IX. Flow Conditions – Papasouliotis and Sotirchos Cases

Papasouliotis and Sotirchos Cases I-III Results

Wall Temperature	Experimental Value	Calculated Value
900 C	0.04 mg/cm^2-min	0.226 mg/cm^2-min
1000 C	0.20 mg/cm^2-min	0.131mg/cm^2-min
1075 C	0.26 mg/cm^2-min	0.129 mg/cm^2-min

Table X. Results – Papasouliotis and Sotirchos Cases

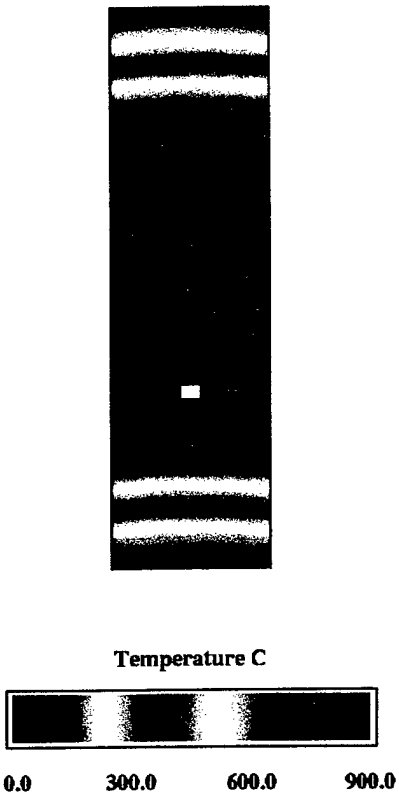

Figure 15. Temperature Contours for Papasouliotis and Sotirchos 900 C case

•CONCLUSIONS

A very general technique has been developed to perform numerical simulation of CVD processes that are commonly used in industry. The numerical technique has been shown to be very robust and is written in a manner such that new physical models can easily be incorporated into the code. A numerical technique has been developed so that very low Mach number-high heat transfer rate cases can be run to convergence in relatively few numbers of iterations, i.e., on the order of 1000-2000 iterations. Wall temperatures of an order of magnitude or more than the free stream temperature can routinely be run at Mach numbers on the order of 10^{-5}. A general homogeneous as well as heterogeneous surface chemistry capability has been developed and demonstrated.

A conjugate heat transfer capability has been couple with the Navier-Stokes solver and results demonstrated for chemically reacting homogeneous as well as heterogeneous surface chemistry for low Mach number-high heat transfer cases with no appreciable increase in the number of iterations needed to obtain a converged solution. Compatibility conditions of temperature and energy balance are satisfied on the surface between the two domains.

A series of six general classes of test cases have been run and results generated. Results have demonstrated that this technique is a viable technique for 'optimizing' a design or evaluating an existing design. When evaluating a present design insight can be gained about the physics of a CVD device that otherwise could not be obtained or if it could be obtained only at a significant cost. Results have been generated and compared with experimental data. The computed results compare favorably with experimental data with respect to obtaining approximate growth rates. However the degree of comparison is not as great as would be desired and further work must be done in this area.

References

1. F. Galasso, Chemical Vapor Deposited Materials, CRC Press, 1991.
2. G. Savage, Carbon-Carbon Composites, Chapman & Hall, 1993.
3. High performance synthetic fibers for composites, A Report of the Committee for National Advisory Board, National Research Council, Publication NMAB-458, National Academy Press, Washington, DC, 1992
4. J.O. Hirschfelder, C.F. Curtiss and R.B. Bird, Molecular Theory of Gases and Liquids, John Wiley & Sons, Inc., 1954.
5. R.B Bird, W.E. Stewart and E.N. Lightfoot, Transport Phenomena, John Wiley & Sons, Inc.,1960.
6. J.D. Ramshaw, Hydrodynamic Theory of Multicomponent Diffusion and Thermal Diffusion in Multitemperature Gas Mixtures, J. *Non-Equilib. Thermodyn.*, 18, p. 121-123 (1993).
7. J.D. Ramshaw, Self-Consistent Effective Binary Diffusion in Multicomponent Gas Mixtures, *J. Non-Equilib. Thermodyn.*, 15, p. 295-300, (1990).
8. J.D. Ramshaw, private communication (1995).
9. M.E. Coltrin, R.J. Kee and F.M. Rupley, SURFACE CHEMKIN (Version 4.0): A Fortran Package for Analyzing Heterogeneous Chemical Kinetics at a Solid Surface - Gas Phase Interface, Sandia Report SAND90-8003B • UC-401, July 1991.
10. S.W. Benson, Thermochemical Kinetics, John Wiley & Sons, 1976.
11. M. Meyyappan, Computational Modeling in Semiconductor Processing, Artech House, 1994, See Chapter 4.
12. W.R. Briley, D.V. Roscoe, H.J. Gibeling, R.C. Buggeln, J.S. Sabnis, P.D. Johnson and F.W. Huber, Computation of Flow Past a Turbine Blade With and Without Tip Clearance, ASME Paper 91-GT-56, June 1991.
13. D.V. Roscoe, R.C. Buggeln, J.A. Foster and H. McDonald, A numerical Investigation of Fluid Flow for Disk Pumping Applications, ASME Paper 88-GT-299, June 1988.
14. F.J. de Jong, J.S .Sabnis, R.C. Buggeln and H. McDonald, Hybrid Navier-Stokes/Monte Carlo Method for Reacting Flow Calculations, *J of Spacecraft and Rockets*, Vol. 29, No. 3, p. 312, May-June 1992.
15. J.S. Sabnis, F.J. de Jong and H.J. Gibeling, A Two-Phase Restricted Equilibrium Model for Combustion of Metalized Solid Propellants, AIAA-92-3509, AIAA/SAE/ASME/ASEE 28th Joint Propulsion Conference and Exhibit, July 1992.
16. D.V. Roscoe and R.C. Buggeln, Development of a Time-Dependent Navier-Stokes Numerical Procedure for the Simulation of Inlet Buzz, SRA Final Report on NASA Contract NAS3-24851, August 1986.

17. R.C. Buggeln, D.V. Roscoe, Y.N. Kim and H. McDonald, Solution of the Navier-Stokes Equations for the Flow In Advanced Labyrinth Seals, AFWAL-TR-85-2038, May 1985.
18. R.C. Buggeln, S. Shamroth, A.I. Lampson and P.G. Crowell, Three-Dimensional (3-D) Navier-Stokes Analysis of the Mixing and Power Extraction in a Supersonic Chemical Oxygen Iodine Laser (COIL) With Transverse I_2 Injection, AIAA 94-2435, 25th AIAA Plasmadynamics and Lasers Conference, June 1994.
19. P.R. Solomon, M.A. Serlo, J.E. Cosgrove, D.S. Pines, Y. Zhao, R.C. Buggeln and S.J. Shamroth, A Coal-Fired Heat Exchanger for an Externally Fired Gas Turbine, *J. of Engineering for Gas Turbines and Power,* Vol. 118, No. 1, January 1996.
20. J.S. Sabnis, S.K. Choi, R.C. Buggeln and H.J. Gibeling, Computation of Two-Phase Shear-Layer Flow Using an Eulerian-Lagrangian Analysis. AIAA Paper 88-3202. January 1988.
21. Y.T. Chan and S.K. Choi, Numerical Simulation of Inductive-Heated Float Zone Growth, *J. Applied Physics*, 1992.
22. M. Meyyappan and R.C. Buggeln, A Process Model for Reactive Ion Etching and Study of the Effects of Magnetron Enhancement, Material Research Society, 1989 Fall Meeting, November 1989.
23. F.J. de Jong and M. Meyyappan, Numerical simulation of silicon carbide chemical vapor deposition, Diamond and Related Materials, Elsevier,(5),1996.
24. W. R. Briley and H. McDonald; *J. Comp. Phys.*, 24-372, 1977.
25. W. R. Briley and H. McDonald; AIAA Paper 79-1445, July 1979.
26. G.D. Papasouliotis and S.V. Sotirchos, Gravimetric Investigation of the Deposition of SiC Films Through Decomposition of Methyltrichlorosilane, *J. Electrochem. Soc.*, 142, p. 3834, (1995).